

Using Neural Network Ensembles to Separate Ocean Biogeochemical and Physical Drivers of Phytoplankton Biogeography in Earth System Models

Christopher Holder¹, Anand Gnanadesikan¹, Marie Aude-Pradal¹

5 ¹Morton K. Blaustein Department of Earth and Planetary Sciences, Johns Hopkins University, Baltimore, MD, United States of America

Correspondence to: Christopher Holder (cholder2@jh.edu)

Abstract. Earth system models (ESMs) are useful tools for predicting and understanding past and future aspects of the climate system. However, the biological and physical parameters used in ESMs can have wide variations in their estimates. Even small changes in these parameters can yield unexpected results without a clear explanation of how a particular outcome was reached. The standard method for estimating ESM sensitivity is to compare spatiotemporal distributions of variables from different runs of a single ESM. However, a potential pitfall of this method is that ESM output could match observational patterns because of compensating errors. For example, if a model predicts overly weak upwelling and low nutrient concentrations, it might compensate for this by allowing phytoplankton to have a high sensitivity to nutrients. Recently, we demonstrated that neural network ensembles (NNEs) are capable of extracting relationships between predictor and target variables within ocean biogeochemical models. Being able to view the relationships between variables, along with spatiotemporal distributions, allows for a more mechanistically based examination of ESM outputs. Here, we investigated whether we could apply NNEs to help us determine why different ESMs produce different spatiotemporal distributions of phytoplankton biomass. We tested this using three cases. The first and second case used different runs of the same ESM, except that the physical circulations differed between them in the first case while the biological equations differed between them in the second. Our results indicated that the NNEs were capable of extracting the relationships between variables for different runs of a single ESM, allowing us to distinguish between differences due to changes in circulation (which do not change relationships) from changes in biogeochemical formulation (which do change relationships). In the third case, we applied NNEs to two different ESMs. The results of the third case highlighted the capability of NNEs to contrast the apparent relationships of different ESMs and some of the challenges it presents. Although applied specifically to the ocean components of an ESM, our study demonstrates that Earth System Modellers can use NNEs to separate the contributions of different components of ESMs. Specifically, this allows modellers to compare the apparent relationships across different ESMs and observational datasets.

30 **1 Introduction**

Earth system models (ESMs) are increasingly used to help us understand how anthropogenic greenhouse gas emissions will affect biological systems and how such changes will feed back on the climate system. Although these methods provide an avenue for examining processes on a global scale, their representations of biological and physical processes

35 of the natural world are limited by imperfect knowledge and the inability to resolve these processes with current
models which require ever increasingly higher computational costs for additional complexity and resolution. As a
result, estimates of critical biological and physical parameters can vary quite substantially. For example, from tracer
experiments in the North Atlantic subtropical gyre, diapycnal diffusivity was estimated between 0.1 to 0.5 cm² s⁻¹
(Ledwell et al., 1998), with similar values having been used in ESMs. Varying the diapycnal diffusivity within this
range in ESMs has been shown to yield different results in the biogeochemical output (Oschlies, 2001; Duteil and
40 Oschlies, 2011). Furthermore, ESMs do not agree about how to represent phytoplankton growth parameters, such as
temperature dependence. In the nine ESMs compared in Laufkötter et al. (2015), the Q₁₀ value describing the
sensitivity of growth rate to 10 degree increases in temperature ranged from 1.68 to 3, with some models varying the
Q₁₀ values based on the size or type of phytoplankton.

45 The uncertainty associated with some ESM parameters can make it difficult to understand why different ESMs may
yield different predictions for biological variables ranging from productivity to carbon uptake. Bopp et al. (2013)
demonstrated that while CMIP5 models showed the same overall global trends under climate change for variables
such as pH, sea surface temperature, O₂, and primary productivity, there were substantial cross-model differences in
O₂ and primary productivity on regional scales.

50 Traditional methods used to estimate the sensitivity of ESMs often compare the spatial distributions of biological and
physical variables from different runs of a single ESM to each other or to observations. However, occasionally changes
in one parameter improve the simulation of one variable while degrading the simulation of another (see for example,
Bahl et al. (2019), their Table 2). Other times, errors in one variable are due to errors in another (i.e., getting a physical
55 front in the wrong place may mean that the biomass has the wrong distribution).

The intent of ESMs is to get the correct spatial distribution both because the correct relationships between
environmental predictors and target variables are being modelled and because the environmental predictors themselves
are correctly modelled. However, it's difficult to know if the correct relationships are indeed being modelled. Thus, a
60 method is needed in which we can evaluate whether different ESMs yield different projections because of fundamental
differences in biogeochemical formulation, or whether such differences are primarily due to differences in physical
circulations and climate sensitivities. Of the potential methods available, neural network ensembles (NNEs) are a
strong candidate. NNEs are a machine learning (ML) technique which use the average of many individual neural
networks (NNs) to predict the outcome of datasets. The objective of this paper is to investigate whether the application
65 of NNEs and sensitivity analyses can provide useful information for determining the most substantial sources of
differences in ESM outputs.

We previously demonstrated that NNEs were able to extract relationships between biological forcings and outputs
within a simplified biogeochemical model (Holder and Gnanadesikan, 2021). NNEs were able to outperform other
70 ML algorithms, such as random forests. More importantly, NNEs also had the benefits of being able to extrapolate

outside the range of the training dataset and to provide a measure of their uncertainty in their predictions. In Holder and Gnanadesikan (2021), we defined two types of relationships between environmental forcings and biological responses: intrinsic and apparent. *Intrinsic* relationships are those where the effect of one predictor variable on an outcome (target variable) can be examined, while maintaining other predictors at a constant level. An example of this would be the results of a laboratory experiment examining how the growth rate of a particular species of phytoplankton depends on different nutrient concentrations, while all other factors remain constant. For ESMs, an example might be the Michaelis-Menten relationships programmed into ESMs that represent how phytoplankton interact with each nutrient. *Apparent* relationships are determined by how the intrinsic relationships interact across space and time, where individual variables are not controlled but may systematically co-vary. An example of this would be the relationships that emerge in the output of ESMs, where the intrinsic relationships programmed into the ESM have interacted with one another across time and space and then had their outputs averaged into monthly-averaged fields. An example of this in the context of real-world environments would be comparing satellite observations of phytoplankton distributions against monthly distributions of nutrients; where low phytoplankton concentrations may result both from low nutrients and high irradiance in the summer in some locations, but also high nutrients and low irradiance in the winter in other locations. As a result, the apparent relationships between nutrients and biomass would not resemble the intrinsic Michaelis-Menten curves coded in the ESM. A proof-of-concept application of NNEs coupled with sensitivity analyses at the end of Holder and Gnanadesikan (2021) demonstrated the ability of NNEs to draw out the co-limitations in a non-linear biogeochemical model and illustrated how these co-limitations differed from the Michaelis-Menten curves programmed into the model.

For this study, we focus on marine phytoplankton physiology, but these approaches are also applicable to other components of ESMs, including atmospheric and terrestrial. In general, there are two primary drivers that lead to differences in how ESMs simulate phytoplankton biogeography: physical forcings and phytoplankton physiology. Insofar as both of these act to affect nutrient cycling they can also act in combination to produce indirect impacts. Before applying this method to outputs of multiple ESMs, we investigate whether the method works well on different runs of a single ESM in which physical parameters are changed to produce different circulations. It is uncertain whether the NNEs are able to pick out the same apparent relationships of the same ESM when there are differences between runs in the physical forcings and intrinsic biological equations (phytoplankton physiology). If different versions of an ESM, which have different circulations, still yield the same apparent relationships between irradiance/nutrients and biomass, it would suggest that circulation changes do not produce new patterns of co-limitation. It is worth noting that we are only stating this in the context of ESMs, as this may not necessarily be true in the real ocean. Furthermore, it would suggest that differences in the apparent relationships of *different* ESMs could be partitioned between those due to different physical circulations and those with different representations of biology. For example, if one uses the apparent relationships from model A to predict the biomass from model B given the environmental parameters from model B, any differences should be due to differences in the biological formulation.

To investigate the extent to which NNEs could characterize differences across ESMs, we explore three cases:

1. We examine an ESM in which biomass is by construction a function of nutrients and irradiance. Using three
 110 different runs of this ESM, we maintain identical intrinsic biological relationships, but vary the physical
 parameters controlling the circulation across the different runs. The objective of the first case is to quantify the
 extent to which differences in physical circulation might affect the apparent relationships between predictor
 (irradiance, nutrient, and temperature) and target (biomass) variables found by NNEs. If models with different
 circulations produce differences in the apparent relationships, this would indicate that differences in circulation
 115 could push the biology into fundamentally new states, i.e., phytoplankton in one location experience new
 combinations of co-limitation or temporal variability (as described by Henson et al. (2021)). However, if the
 NNEs find the same apparent relationships between runs when the physical circulation is changing, this would
 indicate that the primary effect of changing the circulation is simply to change the times and locations where
 different combinations of irradiance and nutrients are found, rather than creating new patterns of co-limitation,
 120 i.e., phytoplankton are governed by the same dynamics/equations regardless of location.
2. We use the same ESM as that of Case 1, except we maintain similar physical circulations between runs and
 change the intrinsic biological relationships (this results in a small change in circulation because within our
 ESM the biological cycle affects physical circulation by changing the absorption of shortwave radiation). The
 objective of the second case is to quantify the ability of NNEs to detect differences in the apparent relationships
 125 when the intrinsic biological relationships between model runs are different and to document the size of those
 differences.
3. For the final case, we look at two *different* ESMs that have different biogeochemical codes but are run within
 the same physical model giving them identical physical circulations. The first ESM follows the framework of
 the ESMs in Cases 1 and 2, where biomass is a function of nutrients. The second ESM allows biomass to be
 130 advected and diffused, making biomass a function of nutrients, irradiance, *and* physical circulation. The
 objective of the third case is to apply the principles from Cases 1 and 2 to more standard ESMs, to quantify the
 extent to which physical circulation contributes to these apparent relationships, and to identify challenges in
 comparing the apparent relationships between ESMs.

2 Methods

135 2.1 Earth System Models – Biogeochemical Codes

In general, ocean biogeochemical components (BCs) of ESMs predict the evolution of phytoplankton biomass, B ,
 using equations that have the general form

$$\frac{\partial B}{\partial t} + \vec{u} * \nabla B = \mu(N, I, T) * B - G(B, ...) + \nabla * \vec{K} * \nabla B \quad (1)$$

where \vec{u} is the three-dimensional velocity field, μ is the phytoplankton growth rate which is a function of nutrients N ,
 irradiance I , and temperature T , $G(B, ...)$ represents the grazing loss rate, which may be a function of phytoplankton
 140 biomass and/or other variables such as temperature or zooplankton concentration, and \vec{K} is the three-dimensional

mixing tensor. Changes in physical parameters (for example changing the values in \vec{K}) would produce changes in transport of biomass. But the associated changes in circulation would also produce changes in other fields, such as N , I , and T (and thus in growth rate μ). Differences in the physical parameters between models will produce both direct differences, due to transport, and indirect differences, due to changes in growth and/or grazing. Additionally, insofar
 145 as the biology affects the absorption of shortwave radiation, it can produce differences in the circulation (Sweeney et al., 2005), although for the simulations in this paper the differences are relatively small.

For this paper, we focus on the ocean BCs run within two ESMs: Biogeochemistry with Light, Iron, Nutrients, and Gases (BLING) and Tracers of Phytoplankton with Allometric Zooplankton (TOPAZ). As described below, BLING
 150 can be thought of as a simplified version of TOPAZ. For Cases 1 and 2, we only use model runs within different versions of GFDL ESM2Mc, in which BLING is the BC, with the reasoning that if the NNEs are unable to distinguish apparent relationships in the simpler BLING model, they would not be able to do so in the more complex TOPAZ model. In Case 3, we use versions of the GFDL ESM2M model in which BLING and TOPAZ are used as the BCs to compare apparent relationships found within the ESM.

155 2.2 Biogeochemistry with Light, Iron, Nutrients, and Gases (BLING)

BLING is a diagnostic biogeochemical model (Fig. 1) described in Galbraith et al. (2010), which was developed as a relatively computationally cheap biogeochemical code that could be run in high-resolution models. Only four explicit tracers are included in the model: oxygen, dissolved organic phosphorus, phosphate, and iron (the last two corresponding to the nutrients (N) in Fig. 1). Phytoplankton are represented as two size classes: small and large
 160 (Biomass (B) in Fig. 1). Phytoplankton growth and grazing $G(B, T)$ are modelled using the phytoplankton size-dependent loss equation developed by Dunne et al. (2005) represented as

$$\mu(N, I, T) * B \approx G(B, T) = \lambda \left(\frac{B}{P_*} \right)^\alpha B \quad (2)$$

where λ is a grazing rate, P_* is a biomass scaling for grazing, and α is a grazing exponent. The grazing rate includes all losses due to grazing, viral lysis, temperature-dependent loss, and others. For the small phytoplankton size class $\alpha = 1$ and for the large phytoplankton size class $\alpha = 1/3$. This means the large phytoplankton biomass is more sensitive
 165 to environmental conditions than the small phytoplankton biomass. The growth rate (μ) in Eq. (2) goes as

$$\mu = \mu_o \cdot \exp(kT) \cdot \left(1 - \exp\left(-\frac{I}{K_I}\right) \right) \cdot \min\left(\frac{Fe}{K_{Fe} + Fe}, \frac{PO_4}{K_{PO_4} + PO_4}\right) \quad (3)$$

where μ is the growth rate, T is the temperature with constant $k = 0.063^\circ\text{C}^{-1}$ following Eppley (1972), $K_{Fe, PO_4, I}$ are the half-saturation constants, and I , Fe , and PO_4 , are the irradiances and the concentrations of dissolved iron and phosphate, respectively. K_I is a function of the nutrient and temperature dependent growth rate following Geider et al. (1997). The time averaged biomass then goes as

$$\bar{B} \approx \left(\frac{\mu}{\lambda} \right)^\frac{1}{\alpha} P_* \quad (4)$$

170 Note that this means that given N , I , and T (all of which are still predicted by the circulation model), the apparent relationships between biomass, nutrients, and irradiance are potentially tightly coupled to the intrinsic relationships governing phytoplankton physiology that determine the growth rate.

2.3 Tracers of Phytoplankton with Allometric Zooplankton (TOPAZ)

175 TOPAZ is a prognostic biogeochemical model included in the Geophysical Fluid Dynamics Laboratory (GFDL) ESM2M (Dunne et al., 2013; Fig. 2). It includes a total of 30 tracers to model cycles such as nitrogen, phosphorus, iron, oxygen, carbon, and others (Nutrients (N) in Fig. 2). TOPAZ models three phytoplankton groups (small, large, and diazotrophic; Biomass (B) in Fig. 2) with irradiance limitation based on the equations of Geider et al. (1997). Additionally, phytoplankton loss/grazing and particle export are modelled using the same size-dependent formulation
180 as those used in Eq. (2), though without imposing the quasi-equilibrium assumption that leads to Eq. (4). TOPAZ differs from BLING in its number of tracers (and associated limitations) and the allowance for advection/diffusion of nutrients and biomass (ΔB_i^{phys} in Fig. 2). This means that the loss rate of phytoplankton in TOPAZ is effectively a function of circulation as well the temperature and biomass-dependent grazing rate, $\lambda \left(\frac{B}{B_*}\right)^\alpha$. This will produce different biomasses in locations that have the same growth rates. Additionally, a key difference between BLING and
185 TOPAZ is that the latter includes denitrification and nitrogen fixation. This then means (as suggested by Tyrrell (1999)) that the nitrogen is the proximate limiting nutrient, while phosphorus is the ultimate limiting nutrient; a distinction that is not made in BLING.

3 Case Descriptions

3.1 Case 1 - Same ESM: Identical Biological Equations, Different Physical Circulations

190 The aim of Case 1 is to quantify the extent to which differences in physical circulations between model runs of the same ESM with identical intrinsic biological relationships could affect the apparent relationships found by NNEs. As stated in Section 2.1, we compare versions of GFDL ESM2Mc in which BLING is configured identically so we can be certain the differences are solely due to circulation changing the environmental conditions, and not the phytoplankton loss rates. Within GFDL ESM2Mc, the nominal resolution is 3 degrees longitudinally and 2 degrees
195 latitudinally, while the vertical resolution has 28 levels. Model runs are initialized with observations and spun up for 1900 years. The final 100 years are used to generate a monthly climatology.

We use three configurations of GFDL ESM2Mc. The three model runs consist of: a standard historical pre-industrial model spin-up (BLING – PI Control), a similar case to the first but where the carbon dioxide concentration is four
200 times higher (BLING – 4x CO₂), and a case similar to the historical spin-up except that the horizontal mixing parameter is three times higher (BLING – 3x Mixing). These model runs are described in greater detail in Gnanadesikan et al. (2013), Pradal and Gnanadesikan (2014), and Bahl et al. (2020). With the standard historical model essentially serving

as a form of a “control,” the two remaining cases allow us to examine if changes in the physical circulation could result in changes to the apparent relationships.

205

The predictor variables for each model run are macronutrient (e.g., phosphate), micronutrient (e.g., dissolved iron), irradiance, and temperature. The target variables are small phytoplankton biomass and large phytoplankton biomass. One NNE is trained for each target variable of each model run for a total of six NNEs in Case 1 (three model runs and two target variables in each run). Details of the NNE training and the construction of the individual NNs making up each NNE can be found in Section 3.4.

210

3.2 Case 2 - Same ESM: Different Diagnostic Biological Equations, Near-Identical Physical Circulations

The purpose of Case 2 is to quantify the differences found by NNEs between the apparent relationships of model runs from the same ESM when the biological equations differ between runs, but the physical circulations are nearly identical.

215

As in Case 1, we use different configurations of ESM2Mc, but this time we keep the physical parameterizations constant but change constants within the BLING BC. We use two model runs: the standard historical pre-industrial model spin-up used in Case 1 (BLING – PI Control) and one with similar distributions to PI Control but different half-saturation coefficients (K_{Fe} and K_{PO4} in Eq. (3)) for small and large phytoplankton (BLING – LgSm). Changing the half-saturation coefficients, which directly affects phytoplankton growth, is analogous to changing the biological equations. Relative to the PI Control, the half-saturation coefficients in LgSm are decreased by $\sqrt{3}$ for small phytoplankton and increased by $\sqrt{3}$ for large phytoplankton. While these changes produce differences in circulation and SST via changing the absorption of shortwave radiation, these differences are small ($R^2 = 0.9949$ for SST between the two model runs). The primary impact of these changes is to affect the distribution of nutrients, as increasing the half-saturation coefficients for large phytoplankton makes it harder for these phytoplankton to grow and efficiently export nutrients.

220

225

The predictor variables for the model runs of Case 2 are the same as those in Case 1 (macronutrient, micronutrient, irradiance, and temperature). Likewise, the target variables are also the same as those in Case 1 (small and large phytoplankton biomass). A total of four NNEs are trained for Case 2 (two model runs and two target variables).

230

3.3 Case 3 - Different ESMs: Prognostic vs. Diagnostic Biological Equations, Identical Physical Circulations

For Case 3, the goal is to examine whether the results from a diagnostic BC from Cases 1 and 2 still hold when a prognostic BC is used. Our goal is to examine any differences in apparent relationships, along with identifying challenges when comparing apparent relationships across more realistic ESMs. In this experiment, the BCs are governed by different biological equations but are run within the same physical model so that the temperatures and irradiance seen by the two BC codes are identical.

235

One of our model simulations uses a version of BLING as the BC, while the other uses TOPAZ. For the BLING model run, the iron concentrations are fixed at their climatological values since this formulation was previously used to develop a model for very high-resolution studies (miniBLING). We use this pair of simulations since the miniBLING code is run in an identical physical circulation to the TOPAZ model run and so the irradiance and temperature experienced by the two model ecosystems are identical. The ESM2M uses a 1 degree latitude/longitude resolution with 50 vertical layers and the model is spun up for 2400 years. These simulations are described in more detail in Galbraith et al. (2015), which shows that BLING and miniBLING yield essentially identical predictions for carbon uptake and ocean deoxygenation under increased CO₂.

The predictor variables for Case 3 are limited to variables that are present in both ESMs: macronutrient, micronutrient, and irradiance. The target variable is total biomass. The biomass is not split into small and large phytoplankton biomass because the miniBLING output only contains total biomass. For consistency, the small and large phytoplankton biomass values in TOPAZ are combined to give total biomass. Two NNEs are trained for Case 3 (two ESM runs and one target variable).

3.4 Neural Network Ensembles (NNEs)

NNEs are an ensemble ML method. NNEs are comprised of a collection of individual neural networks (NNs) where the predictions of each NN are averaged into a single prediction. This ensemble approach has been shown to outperform individual NNs and reduce the generalization error within a dataset (Hansen and Salamon, 1990) by turning individual “weak learners” into a single “strong learner.” Individual NNs can fit a non-linear function to a dataset without assuming any prior knowledge of the system. For a more thorough discussion of NNs, please refer to Schmidhuber (2015). The basic structure of the NN approach that we use here is described in Appendix 1 of Scardi (1996).

260

We use NNEs for several reasons:

1. The ensemble approach of NNEs allows us to view the uncertainty in any given prediction based on the individual predictions of each NN.
2. NNEs possess some capability of extrapolating outside the range of the data on which they are trained (Holder and Gnanadesikan, 2021).
3. As recently shown in Holder and Gnanadesikan (2021), NNEs were able to more closely reproduce the underlying intrinsic relationships compared to random forests, mainly because of their ability to extrapolate.

The structure of the individual NNs is consistent between the three cases with each NN containing 25 nodes in the hidden layer with a hyperbolic tangent sigmoid activation function and 1 node in the output layer with a linear activation function. We demonstrated in previous work that the NNE predictions were not greatly improved with the addition of a second hidden layer or with hidden layer node quantities greater than 25 (Holder and Gnanadesikan, 2021). Additionally, the activation function of the hidden layer nodes did not see a substantial increase in performance

275 either as long as a non-linear function was used (Holder and Gnanadesikan, 2021). The settings specified here allow
for reasonable training times while maintaining high performance metrics relative to the other formulations tested in
our previous work (Holder and Gnanadesikan, 2021). For more detailed information, see Appendix B2 in Holder and
Gnanadesikan (2021).

280 The difference between each case is in the number of input nodes: Cases 1 and 2 each contain four input nodes (one
for each predictor) and Case 3 has three input nodes. The predicted concentration of each target variable (second
column of Table 1) in individual NNs can be thought of as a function of the respective predictors (first column of
Table 1). For example, one NN of the NNE for the small phytoplankton biomass target variable in Case 1 would have
the following structure:

1. The four predictor variables for Case 1 (first column of Table 1) correspond to the four nodes in the input layer
285 of the NN.
2. Each of the four input nodes is connected by weights to each of the 25 nodes in the hidden layer. Additionally,
a bias term is connected to each of the hidden nodes.
3. Each of the nodes in the hidden layer is connected by weights to the single node in the output layer, which, for
this instance, would correspond to the target variable of small phytoplankton biomass. As with the hidden layer,
290 a bias term is connected to the single output node.

The training of each NN is carried out using the “feedforwardnet” function in MATLAB 2019b (MATLAB, 2019).
For each trained NN, the “feedforwardnet” function is provided the training dataset, which it then automatically
separates into training, validation, and testing *subsets*, with 70% of the observations from the training dataset going
295 to the training *subset*, 15% to the validation *subset*, and 15% to the testing *subset*. The training stops when the error
between the predictions and observations increases for six consecutive epochs.

300 Separate NNEs are trained for each response variable in each model run, which equates to six NNEs (2 target variables,
3 simulations) in Case 1, four NNEs in Case 2, and two NNEs in Case 3. For consistency, the same framework and
settings are used for the construction of the NNEs with each one consisting of 25 individual NNs.

Each variable is also scaled between -1 and 1 relative to each variable’s maximum and minimum

$$V_S = \frac{\max_S - \min_S}{\max_U - \min_U} (V_U - \min_U) + \min_S \quad (5)$$

305 Where V is the value of a variable being scaled, S (subscript) is the scaled value, and U (subscript) is the unscaled
value. This scaling puts the predictor values in the same range, so more weight is not given to variables with larger
ranges. Additionally, this step decreases the training time of the NNs so that no values are too close to the limits of
the hyperbolic tangent sigmoid activation function. The variables and predictions are then scaled back to their original
values for analysis and presentation of the results (Eq. (6)). The letter representations in Eq. (6) are the same as those
in Eq. (5).

$$V_U = \frac{\max_U - \min_U}{\max_S - \min_S} (V_S - \min_S) + \min_U \quad (6)$$

310 When using ML, it is possible to produce overly complex relationships that “overfit” the data. This provides a good
 match for the data on which an ML model is trained but leads to poor predictions when new data is presented to the
 model. This can be avoided by splitting a dataset into training and testing subsets. For this manuscript, this means
 each NNE is trained using only the observations in the training subset and tested on the observations from the testing
 subset. The data from each model run is randomly split into training and testing subsets with 60% of the observations
 315 from a dataset going to the training subset and the other 40% going to the testing subset. The observations set aside in
 the testing subset are ones that the NNEs never see during their training phase. This provides a way to evaluate each
 trained NNE and its generalizability. If performance metrics of a trained NNE are similar between the training and
 testing subsets, it suggests that the variance of the dataset is well captured in the training phase and the NNE is
 generalizable to the entire dataset.

320 To assess the performance of each NNE, we calculate the standard R^2 values and root mean squared error (RMSE) by
 comparing the monthly biomass predictions from each NNE to the “true” monthly biomass values of the model runs
 within the respective training and testing subsets.

325 The NNEs in each case and matching size class are also asked to make predictions on the testing subsets of the other
 model runs. For example, in Case 1 the NNE trained on the small phytoplankton of PI Control is asked to make
 predictions for small phytoplankton of 4xCO₂ using the values of the predictors from the testing subset of the 4xCO₂
 model run. These results are then compared to the actual values of the target variable to calculate the RMSE. This
 RMSE is then used to calculate the percent increase/decrease in error when compared against the RMSE calculated
 330 from a point-by-point comparison of each model run against the others. The purpose of this is to provide another
 metric for testing if the NNEs are finding common apparent relationships across model runs. If an NNE trained on
 one model run is able to predict the outcomes of the other model runs with errors that are similar in magnitude to the
 NNEs that were trained on those runs, it would suggest that the NNEs are finding similar apparent relationships
 between the model runs. On the other hand, if it shows an increase in RMSE, it suggests that the apparent relationships
 335 between the model runs are different in biologically important ways.

To view the apparent relationships found by the NNEs, we conduct sensitivity analyses in which we present each NNE
 with a unique set of values for the predictors. Compared to spatiotemporal distributions and time series, sensitivity
 analyses allow for the visualization of relationships between predictor and target variables. In each sensitivity analysis,
 340 one predictor is varied across its minimum and maximum range, while the other variables are held at a specified value,
 such as each variable’s 25th percentile. This is repeated for the 50th and 75th percentile values of each variable as well.
 This allows us to visualize how the biomass predictions change across one variable’s range when the other variables
 are held at a specified value. An example of this is varying the macronutrient concentration while holding the

micronutrient, irradiance, and temperature variables at their 25th or 75th percentile values. This allows us to see how
345 the macronutrient concentration affects biomass when other nutrients are low or high, respectively.

4 Results and Discussion

4.1 Case 1 – Same ESM: Identical Biological Equations, Different Physical Circulations

In Case 1, our objective is to quantify the extent to which differences in physical circulation might affect the apparent
relationships found by NNEs when the intrinsic biological relationships remain the same between the model runs and
350 the physical circulation parameters differ. It is uncertain whether changing the circulation would lead to new patterns
of co-limitation (i.e., different apparent relationships) or whether the physical circulation would simply act to change
the location of where combinations of irradiance and nutrients are found (i.e., same apparent relationships).

Our results support the latter outcome, that the locations of particular environments are simply being shuffled around.
355 The sensitivity analysis shows that each NNE finds similar apparent relationships between biomass and each of the
predictors for the respective size classes, insofar as each line falls within the standard deviation of the others (Fig. 3
and 4). For example, the standard deviation (gray region) around the predicted apparent relationships for the large
phytoplankton (dashed lines) all overlap one another (Fig. 3). The same is seen for the predicted apparent relationships
for the small phytoplankton (Fig. 4). Additionally, we are confident in the apparent relationships since each NNE
360 acquires high performance metrics in both the training and testing subsets (highest RMSE = 3.11×10^{-9} mol P kg⁻¹;
Table 2) relative to the mean value of the total biomass (1.24×10^{-8} mol P kg⁻¹).

This result can be better understood by considering the conceptual diagram of how the diagnostic BC BLING works
within an ESM (Fig. 1). For each time step, nutrients are calculated as a function of three terms: the initial nutrients,
365 the change in nutrients from biology, and the change in nutrients from physical circulation. In contrast, the biomass is
only a function of two terms: the initial biomass values and the change in biomass due to biological cycling. Thus,
biomass is not directly affected by changes in the physical circulation. Additionally, this means that when given
information on the biological predictors, but not the physical parameters, the NNEs are able to back out the apparent
relationships quite well. Although it would seem obvious from Fig. 1 that the biomass is not directly affected by
370 changes in the physical circulation, we were unsure whether indirect impacts of such changes (changing patterns of
co-limitation or temporal variability) would affect the results. Our results indicate that such indirect effects were absent
or, at most, minor.

That similar apparent relationships are found between the model runs is further supported when we task each trained
375 NNE with making predictions on the testing subsets of the other model runs for the same size class. For example, the
NNE trained on the PI Control for small phytoplankton can be tasked with making predictions for the small
phytoplankton biomass of 4xCO₂ and 3xMixing using the predictor values from their testing subsets. This test allows
for the evaluation of the robustness of the relationships that each NNE finds. If the NNEs are finding different

relationships between the model runs, the NNE from one model run will likely perform poorly when predicting the other model runs. Our results show that the NNEs perform well when applied to the other model runs (highest RMSE = 3.74×10^{-9} mol P kg^{-1} ; Table 3) relative to the average value of total biomass (1.24×10^{-8} mol P kg^{-1}). Given that these values are close to the performance metrics of their original datasets (Table 2 vs Table 3), it seems logical to say that this is because they are finding the same relationships.

385 Additionally, using the NNEs to predict the other runs leads to decreases in error relative to the error from comparing each run against the others. For example, the initial point-by-point comparison of 4xCO₂ and PI Control for small phytoplankton (Fig. 5 d) shows an RMSE of 3.06×10^{-9} mol P kg^{-1} , while using the NNEs from each model run to predict the other saw the RMSE go down with a reduction in error of about 76% (Table 3). This reduction of error is consistent across the other model runs and size classes with error reductions varying from 54-79% (Table 3). This implies the NNEs applied to the other runs are better able to predict the outcome than the point-by-point analysis, once again reinforcing our previous result.

That the NNEs from one model run are able to reproduce the results from the other model runs is not simply due to the models producing similar spatiotemporal patterns. To ensure that distinct differences between the model runs are present, we compare each model run against the others (Fig. 5 and 6). Differences in the biomass values between the three model runs are evident (Fig. 5 and 6). First, we compare each model run against the others in a point-by-point analysis and observe that different biomasses are occurring at the same spatiotemporal locations (Fig. 5 and 6 d, g, h). For example, in the small phytoplankton scatter plot for PI Control vs 4xCO₂, PI Control shows a tendency of having higher biomass values than 4xCO₂ across most locations (Fig. 5 d). Additionally, we look at the contour plots and log₁₀ relative ratios using the yearly averaged biomass for each case (Fig. 5 and 6 a-c, e, f, i). Specific large differences that we note are higher biomass in the Pacific and Northern Atlantic in PI Control and 3xMixing relative to 4xCO₂ (Fig. 5 and 6 b, f) and the highest biomass occurring in 3xMixing in the subtropical regions of the Pacific (Fig. 5 and 6 c). Similar patterns are observed in the large phytoplankton, as well (Fig. 6). These differences between the model runs are relatively large (exceeding a factor of three in some locations) and allow us to dismiss the possibility that the similar apparent relationships are only due to strong similarities between the model runs.

Although the sensitivity analysis allows us to see that the apparent relationships were the same for each size class, it also allows us to see how the two size classes react differently to the same conditions. Most notably, the large phytoplankton seem to be very sensitive to the micronutrient compared to the small phytoplankton (Fig. 3; closer view of small phytoplankton in Fig. 4). When the other predictors are held at their 75th percentile values (high macronutrient, high irradiance, and warm temperature), the large phytoplankton reach biomass values almost an order of magnitude higher than the small phytoplankton (Fig. 3 and 4 j). This is what would be expected given the cubic relationship of large phytoplankton with growth rate. Another interesting relationship is the stark asymptotes in both size classes of the macronutrient plots, suggesting limitations by other nutrients, likely the micronutrient (Fig. 3 a, e, i). One unexpected relationship is the decreasing biomass with increasing temperature in both size classes (Fig. 3 d, h, l). This

could be a result of warmer regions having less available nutrients or because of the temperature dependent chlorophyll-to-carbon (Chl:C) ratios (Geider et al., 1997) which would lead to phytoplankton needing higher irradiance in warmer waters.

420 Relative to our main objective in Case 1 to quantify the extent to which differences in physical circulation affect the apparent relationships, our results indicate that the different physical circulations do not produce differences in the apparent relationships found by NNEs. When the biological equations remain the same, changing the physical parameters simply changes where combinations of nutrients and irradiance occur. The NNEs can find the same apparent relationships between the model runs when the equations and constants governing those runs are identical,
425 even if the inputs differ. In contrast to changes in nutrients, changes in biomass in the BLING ESM are not a function of the physical circulation.

4.2 Case 2 – Same ESM: Different Diagnostic Biological Equations, Near-Identical Physical Circulations

430 In Case 1, it is clear from our results that when the biological cycling is identical between model runs, the NNEs find the same apparent relationships because the biomass is not a function of the physical circulation. Since the biomass is clearly a function of the biological equations, it would be reasonable to assume that the apparent relationships could be different between model runs that are governed by different biological equations. So, for Case 2, the objective is to quantify the extent to which NNEs can detect differences in the apparent relationships when the intrinsic biological
435 relationships between model runs are different, while maintaining similar physical circulations and still using a diagnostic model which guarantees that identical nutrient, irradiance, and temperature at two different points will produce identical biomass.

Our results show that NNEs can differentiate the apparent relationships between model runs when the biological
440 equations differ. The sensitivity analysis for Case 2 shows that different apparent relationships are found between model runs and within the same size classes, relative to the non-overlapping gray standard deviation regions around each line (Fig. 7 and 8). Additionally, we can be fairly confident in these predictions given the high-performance metrics in both the training and testing subsets (highest RMSE = 3.11×10^{-9} mol P kg⁻¹ [Table 2] vs. the average total biomass of 1.36×10^{-8} mol P kg⁻¹).

445 This result of different relationships, when the model runs are governed by different biological equations, reinforces what we found in Case 1. Changing the biological equations can be likened to changing how the nutrients affect the phytoplankton biomass (the function $g(N_{j,L1,L2})$ in Fig. 1). While it might seem obvious that changing the biological equations will change the biomass values, it remains unclear whether NNEs would be able to pick out these differences
450 in the apparent relationships.

We want to ensure there are noticeable differences between the model runs (Fig. 9 and 10). We did this in Case 1 to ensure that the similar apparent relationships found by the NNEs were not simply because of similarities in the model output. In Case 2, the difference in model outputs serves to reinforce the different apparent relationships found by the NNEs. In the point-by-point comparison, the large phytoplankton show more agreement between model runs (Fig. 10 c) than the small phytoplankton (Fig. 9 c). However, when we examine the contour and log10 relative ratios (Fig. 9 and 10 a, b, d), it is evident that large, systematic, spatially coherent differences exist between the model runs. Both the small and large phytoplankton show higher concentrations in the LgSm model run compared to PI Control for the subtropical and polar regions of the Pacific and Indian Oceans, along with higher concentrations in the equatorial Atlantic (Fig. 9 and 10).

Although the gray regions in Figs. 7 and 8 overlap toward the higher concentrations of each predictor, this is likely due to the lack of observations in the training data meeting those criteria, without which the NNEs cannot be constrained. For example, in Fig. 7 (j), the apparent relationships of the large phytoplankton overlap past about 5×10^{-10} mol kg⁻¹ of the micronutrient, because there are no observations in the training data that are greater than 5×10^{-10} mol kg⁻¹ of the micronutrient while simultaneously being at the 75th percentile level of the macronutrient, irradiance, and temperature (data not shown). Without observations to constrain them, the NNEs cannot be constrained and, therefore, are less certain about the extrapolated relationships in those regions which leads to higher uncertainty and overlapping standard deviations.

As in Case 1, our result is supported by the additional test in which the NNEs trained on one model run are tasked with making predictions on the other. Had the NNEs found similar apparent relationships, the reductions in error would have been of similar magnitude as those in Case 1 (Table 3 vs Table 4). For this second case, we see that there are only modest decreases in RMSE for the small phytoplankton and increases in RMSE for large phytoplankton (Table 4). For example, relative to the RMSE of the point-by-point comparison, the RMSE decreases about 21% when LgSm makes predictions on PIControl for the small phytoplankton (Table 4). Additionally, it is observed that even though the RMSE increases in the large phytoplankton, the R² values improve in the cross-model comparison compared to the point-by-point comparison (0.92-0.93 vs 0.85; Table 4). This suggests that the NNEs improve the simulation in terms of the overall pattern, but not the magnitude. These results make sense since the apparent relationships of the small phytoplankton show greater similarities than the apparent relationships of the large phytoplankton (Fig. 7).

With respect to the apparent relationships that the NNEs uncover, the large phytoplankton once again appear to be more sensitive to the micronutrient concentrations compared to the small phytoplankton (Fig. 7 b, f, j). Both size classes show asymptotes around the same concentrations for the macronutrient, albeit at different biomass values (Fig. 7 a, e, i). As with Case 1, the decreasing biomass with increasing temperature is an unexpected relationship (Fig. 7 d,

h, l), which might be explained by the temperature dependent Chl:C ratios causing phytoplankton in warmer regions to need higher irradiance.

490 As previously stated, our main objective with Case 2 is to quantify the extent to which NNEs can detect differences in the apparent relationships when the physical conditions between model runs are identical and the biological relationships differ. With the biomass being a function of changes in biomass from biology (i.e. the equations governing how nutrients affect biomass), it is unsurprising that different biological equations produce differences in biomass. What was unclear was whether NNEs would be able to highlight these differences in the apparent
495 relationships. Our results indicate that NNEs can find noticeable differences in the apparent relationships, insofar as the standard deviation region of the sensitivity analysis curves do not overlap.

4.3 Case 3 – Different ESMs: Prognostic vs. Diagnostic Biological Equations, Identical Physical Circulations

From Cases 1 and 2, we learn from our results that NNEs are capable of discerning differences in apparent relationships between model runs of the same ESM. For Case 3, we apply these principles to different ESMs to quantify the
500 differences in the apparent relationships and highlight challenges that arise in comparing relationships between ESMs. The model runs of Cases 1 and 2 using BLING as a BC affords us the opportunity to test a “best-case” scenario for predicting biomass from nutrients and irradiance because of the tight coupling of growth rate and biomass (i.e., knowing the growth rate means we know the biomass). In Case 3, the ESMs have different biogeochemical codes (i.e., different biological equations) and identical physical circulations. One ESM (ESM2Mo with miniBLING as BC,
505 referred to as miniBLING) is comparable to the BLING formulation in that the growth rate is tightly coupled with the biomass. However, the other ESM (ESM2Mo with TOPAZ as BC, referred to as TOPAZ) does not have as tight of a coupling. The TOPAZ simulation allows biomass to be advected and diffused in the same way as nutrients, effectively making biomass a function of nutrients and physical circulation, which is more typical of ESMs and likely true in the real ocean, as well.

510 Our results indicate that the phytoplankton in the two ESMs react differently to the same conditions. It should be noted that total phytoplankton biomass is used for Case 3, rather than splitting the biomass into large and small because phytoplankton output by the miniBLING BC is not differentiated into size classes. The sensitivity analysis shows that the miniBLING simulation produces higher biomass concentrations than the TOPAZ simulation under the same
515 conditions (Fig. 11), except at lower concentrations of nutrients where they seem to react similarly (Fig. 11 a, b, c). This is not entirely unexpected since the biomass values in the miniBLING simulation are generally much higher than those in the TOPAZ simulation, as can be seen in the point-by-point comparison (Fig. 12 c). However, not all the biomass values in the miniBLING simulation are larger than those in the TOPAZ simulation. The subtropical Atlantic regions and northern subtropical Pacific have higher yearly averaged biomass values in the TOPAZ simulation
520 compared to the miniBLING simulation (Fig. 12 a, b, d). As with Case 2, the additional test of asking the NNEs trained on the output of one ESM to predict the output from the other ESM reinforces the result that different apparent relationships are found from an increase in error for both ESMs (Table 5).

The challenge of comparing the results of different ESMs is evident in Case 3. For example, the performance metrics for the model runs in Cases 1 and 2 are relatively high in both the training and testing subsets, but the performance metrics for the TOPAZ simulation in Case 3 are much lower ($R^2 > 0.97$ vs ~ 0.58 , respectively; Table 2). From these results alone, it is unclear whether this drop in performance is because we are unable to characterize the TOPAZ simulation with NNEs using predictors common to both runs or whether we simply do not include enough relevant variables. To understand this, we perform a brief analysis in which we train NNEs on specific variables and measure their performance with ESM output from CMIP5 ESM2M, which has TOPAZ as its BC (Table 6). One NNE is trained using only variables that directly affected the phytoplankton growth rate (biology), one is trained using only variables that do *not* directly affect the growth rate (physics), and another is trained with both sets of variables (all). Our results indicate that we are able to characterize ESM2M (and, by extension, results produced by using TOPAZ as a BC) with NNEs with the inclusion of more relevant variables, such as nitrate, ammonium, and silicate (RMSE $\sim 5.90 \times 10^{-5}$ mol N m^{-3} [Table 6] vs. the average biomass value of 3.14×10^{-4} mol N m^{-3}). Without the inclusion of all the relevant variables as predictors, the performance of the NNE trained on output from the TOPAZ simulation suffers compared to the NNE trained on the miniBLING simulation.

An additional challenge with comparing different ESMs is that certain variables may not be present in all ESMs. For example, one ESM may have phosphate included as a variable and another ESM may not. This presents a problem when using the sensitivity analyses, because each NNE needs to be presented with the same conditions for direct comparability. One potential method for mitigating this could be to use proxy-variables, such that variables not common to both ESMs could be modified to represent the missing variables. For example, if one ESM has phosphate as a variable and another ESM does not, it might be possible to modify a variable that would be equivalent to phosphate, such as nitrate. Using the Redfield ratio of 16:1 for the N:P ratio, the nitrate variable could be divided by 16 and thus be considered a proxy variable for phosphate. This proxy phosphate variable could then be used in training the NNE particular to the applicable ESM, so all NNEs would be trained using the same predictors.

5 Summary and Conclusions

A challenge of using ESMs is understanding why different ESMs yield different results, even when they are run under similar conditions. Our objective with this manuscript was to investigate the extent to which NNEs could characterize differences across ESMs through differences in circulation vs differences in biological formulations. We approached this objective by exploring three cases:

1. In the first case, we compared three configurations of an ESM that had identical intrinsic biological relationships but different physical circulations. The purpose of this case was to quantify the extent to which differences in physical circulations between model runs of the same ESM could affect the apparent relationships found by NNEs.

2. In the second case, we compared two model runs from the same ESM, except that the intrinsic biological equations were different, and the physical circulations were similar. The purpose of this case was to quantify the extent to which NNEs found differences in the apparent relationships and the size of those differences.
- 560 3. In the third case, we used two different ESMs that had different intrinsic biological relationships but identical physical circulations. The greatest difference between them was that in one ESM (ESM2Mo with TOPAZ as BC), biomass was able to be advected and diffused making it a function of nutrients, irradiance, *and* circulation. This was in contrast to the other ESM (ESM2M with miniBLING embedded as BC) where biomass was only a function of nutrients. The purpose of this case was to apply what we had learned in the first two cases to a
- 565 more realistic ESM to quantify differences in the apparent relationships and identify any challenges.

Our results indicated that when all the relevant variables were included as predictors, the NNEs served as a parsimonious representation of the ESMs. With the first and second cases, NNEs were able to attribute differences between the model runs to physics and biological factors, respectively. The third case demonstrated that NNEs could

570 be used to compare apparent relationships between different ESMs and find their key differences, along with highlighting some of the challenges in applying this to more realistic models.

The results of our study suggest that oceanographers and climate scientists could use the methods we have demonstrated to compare apparent relationships between ESMs, in addition to using spatiotemporal distributions and

575 time series. This is not to say that spatiotemporal information is not important; rather, the relationships and spatiotemporal information can be used to inform one another. For example, in a side-by-side comparison of contour plots between biomass and nitrate concentrations, one might expect to see high biomass in high nitrate regions. However, if low biomass is observed in a high nitrate region, this would suggest that another factor (such as phosphate) is limiting phytoplankton growth. By visualizing the apparent relationships, one would be able to observe that

580 phosphate has a strong limitation factor on the phytoplankton. This could then be verified with the spatial contour plot of phosphate against the original biomass and nitrate contour plots.

In addition to comparing relationships between ESMs, the methods presented here can allow for the comparison of relationships found in observational datasets to the relationships in ESMs, allowing for better tuning of the models

585 and more accurate representations of the natural world and what changes we might expect under climate change. Our results here show the “best case” for comparing models with observations. The prevailing assumption is that environmental conditions set biomass and that ecological details do not matter; if two places have the same nutrients, irradiance, and mixing, they will have the same phytoplankton biomass. Our methods demonstrate that we can evaluate the extent to which such dynamics usually hold. In a follow-up paper, our preliminary results show that these methods

590 can explain a large portion of the variance (60-80%) in two satellite-derived observational datasets, along with greater than 90% across a suite of CMIP6 ESMs.

Appendix A

This appendix provides additional information about the datasets used in each of the three cases, along with information about how each dataset was randomly sampled.

595

The sizes of the datasets were as follows: 77,328 datapoints for each model run in Case 1, 77,328 datapoints for each model run in Case 2, and 577,332 datapoints for each model run in Case 3. Each dataset was split into training and testing subsets with 60% of the full dataset going to the training subset and 40% going to the testing subset. The training subset for each model run contained 46,397 datapoints in Case 1, 46,397 datapoints in Case 2, and 364,399
600 datapoints in Case 3. The testing subsets for each model run contained 30,932 datapoints in Case 1, 30,932 datapoints in Case 2, and 230,934 datapoints in Case 3.

605

The composition of the training and testing subsets were determined by random sampling, such that they randomly sampled the full dataset in both space and time. Specifically, the random number generator function for MATLAB, 2019b was set to “twister” and the seed was set as “123” for reproducibility. Each datapoint was either part of the training subset or the testing subset; no observations were part of both.

Code Availability

610 The Matlab scripts (MATLAB, 2019) for processing the outputs of the ESM model runs, training the NNEs, and
constructing the tables and figures are available in the following Zenodo repository:
<https://doi.org/10.5281/zenodo.4774437> (Holder et al., 2021).

Data Availability

615 The output of the ESM model runs (which serve as the input for training the NNEs) for each case are available in the
following Zenodo repository: <https://doi.org/10.5281/zenodo.4774437> (Holder et al., 2021).

Author contribution

620 The conceptualization and methodology of the research was developed by CH and AG. The coding scripts that
configured the data for training, trained the NNEs, and produced the tables/figures were written by CH. The analysis
and interpretation of the data was carried out by CH and AG. AG and MAP ran the ESMs that produced the model
output for Cases 1 and 2. MAP coded the LgSm version of the BLING BC used in Case 2. The original draft of the
manuscript was written by CH and AG, with edits, suggestions, and revisions provided by MAP.

Competing Interests

The authors declare that they have no conflicts of interest.

Financial Support

625 This research was supported by the National Science Foundation Division of Ocean Sciences (Grant No. 1756568),
the Department of Energy (Grant No. DE-SC0019344) and the National Oceanographic and Atmospheric
Administration (Grant No. NA21OAR4310256).

References

- Bahl, A., Gnanadesikan, A., and Pradal, M.-A. (2019). Variations in Ocean Deoxygenation Across Earth System
630 Models: Isolating the Role of Parameterized Lateral Mixing. *Glob. Biogeochem. Cycles* 33, 703–724.
doi:10.1029/2018GB006121.
- Bahl, A., Gnanadesikan, A., and Pradal, M.-A. S. (2020). Scaling Global Warming Impacts on Ocean Ecosystems:
Lessons From a Suite of Earth System Models. *Front. Mar. Sci.* 7. doi:10.3389/fmars.2020.00698.
- Bopp, L., Resplandy, L., Orr, J. C., Doney, S. C., Dunne, J. P., Gehlen, M., et al. (2013). Multiple stressors of ocean
635 ecosystems in the 21st century: projections with CMIP5 models. *Biogeosciences* 10, 6225–6245.
doi:10.5194/bg-10-6225-2013.
- Dunne, J. P., Armstrong, R. A., Gnanadesikan, A., and Sarmiento, J. L. (2005). Empirical and mechanistic models for
the particle export ratio. *Glob. Biogeochem. Cycles* 19. doi:https://doi.org/10.1029/2004GB002390.
- Dunne, J. P., John, J. G., Shevliakova, E., Stouffer, R. J., Krasting, J. P., Malyshev, S. L., et al. (2013). GFDL’s ESM2
640 Global Coupled Climate-Carbon Earth System Models. Part II: Carbon System Formulation and Baseline
Simulation Characteristics*. *J. Clim.* 26, 2247–2267. doi:10.1175/JCLI-D-12-00150.1.
- Duteil, O., and Oschlies, A. (2011). Sensitivity of simulated extent and future evolution of marine suboxia to mixing
intensity. *Geophys. Res. Lett.* 38. doi:https://doi.org/10.1029/2011GL046877.
- Eppley, R. W. (1972). Temperature and phytoplankton growth in the sea. *Fish. Bull.* 70, 1063–1085.
- 645 Galbraith, E. D., Dunne, J. P., Gnanadesikan, A., Slater, R. D., Sarmiento, J. L., Dufour, C. O., et al. (2015). Complex
functionality with minimal computation: Promise and pitfalls of reduced-tracer ocean biogeochemistry
models. *J. Adv. Model. Earth Syst.* 7, 2012–2028. doi:10.1002/2015MS000463.
- Galbraith, E. D., Gnanadesikan, A., Dunne, J. P., and Hiscock, M. R. (2010). Regional impacts of iron-light
colimitation in a global biogeochemical model. *Biogeosciences* 7, 1043–1064.
650 doi:https://doi.org/10.5194/bg-7-1043-2010.
- Geider, R. J., MacIntyre, H. L., and Kana, T. M. (1997). Dynamic model of phytoplankton growth and acclimation:
responses of the balanced growth rate and the chlorophyll a: carbon ratio to light, nutrient-limitation and
temperature. *Mar. Ecol. Prog. Ser.* 148, 187–200.
- Gnanadesikan, A., Bianchi, D., and Pradal, M.-A. (2013). Critical role for mesoscale eddy diffusion in supplying
655 oxygen to hypoxic ocean waters. *Geophys. Res. Lett.* 40, 5194–5198. doi:https://doi.org/10.1002/grl.50998.

- Hansen, L. K., and Salamon, P. (1990). Neural network ensembles. *IEEE Trans. Pattern Anal. Mach. Intell.* 12, 993–1001. doi:10.1109/34.58871.
- Henson, S. A., Cael, B. B., Allen, S. R., and Dutkiewicz, S. (2021). Future phytoplankton diversity in a changing climate. *Nat. Commun.* 12, 5372. doi:10.1038/s41467-021-25699-w.
- 660 Holder, C., and Gnanadesikan, A. (2021). Can machine learning extract the mechanisms controlling phytoplankton growth from large-scale observations? – A proof-of-concept study. *Biogeosciences* 18, 1941–1970. doi:10.5194/bg-18-1941-2021.
- Holder, C., Gnanadesikan, A., and Pradal, M.-A. (2021). Dataset and scripts for manuscript “Using Neural Network Ensembles to Separate Ocean Biogeochemical and Physical Drivers of Phytoplankton Biogeography in Earth
- 665 System Models.” Zenodo. doi:10.5281/zenodo.4774437.
- Laufkötter, C., Vogt, M., Gruber, N., Aita-Noguchi, M., Aumont, O., Bopp, L., et al. (2015). Drivers and uncertainties of future global marine primary production in marine ecosystem models. *Biogeosciences* 12, 6955–6984. doi:https://doi.org/10.5194/bg-12-6955-2015.
- Ledwell, J. R., Watson, A. J., and Law, C. S. (1998). Mixing of a tracer in the pycnocline. *J. Geophys. Res. Oceans*
- 670 103, 21499–21529. doi:https://doi.org/10.1029/98JC01738.
- MATLAB version 9.7.0.1319299 (R2019b) Update 5 (2019). Natick, Massachusetts: The Mathworks, Inc.
- Oschlies, A. (2001). Model-derived estimates of new production: New results point towards lower values. *Deep Sea Res. Part II Top. Stud. Oceanogr.* 48, 2173–2197. doi:10.1016/S0967-0645(00)00184-3.
- Pradal, M.-A., and Gnanadesikan, A. (2014). How does the Redi parameter for mesoscale mixing impact global
- 675 climate in an Earth System Model? *J. Adv. Model. Earth Syst.* 6, 586–601. doi:https://doi.org/10.1002/2013MS000273.
- Scardi, M. (1996). Artificial neural networks as empirical models for estimating phytoplankton production. *Mar. Ecol. Prog. Ser.* 139, 289–299.
- Schmidhuber, J. (2015). Deep learning in neural networks: An overview. *Neural Netw.* 61, 85–117.
- 680 doi:10.1016/j.neunet.2014.09.003.
- Sweeney, C., Gnanadesikan, A., Griffies, S. M., Harrison, M. J., Rosati, A. J., and Samuels, B. L. (2005). Impacts of Shortwave Penetration Depth on Large-Scale Ocean Circulation and Heat Transport. *J. Phys. Oceanogr.* 35, 1103–1119. doi:10.1175/JPO2740.1.

Tyrrell, T. (1999). The relative influences of nitrogen and phosphorus on oceanic primary production. *Nature* 400, 685–689. doi:10.1038/22941.

Tables

Table 1: Summary of each case which includes information on the predictor variables, the target variables, the ESMs, the model runs, the biological specifications, and the physical circulation specifications.

Case #	Predictor Variables	Target Variables	Biogeochemical Component	Model Runs	Biological Specifications	Physics/Circulation Specifications
1	Macronutrient (mol kg^{-1}); Micronutrient (mol kg^{-1}); Irradiance (W m^{-2}); Temperature ($^{\circ}\text{C}$)	Small Phytoplankton Biomass (mol P kg^{-1}); Large Phytoplankton Biomass (mol P kg^{-1})	BLING	PI Control; 4xCO ₂ ; 3x Mixing	Identical diagnostic BC across model runs	Predicted by different versions of ESM2Mc produced by significant changes in physical parameters
2	Macronutrient (mol kg^{-1}); Micronutrient (mol kg^{-1}); Irradiance (W m^{-2}); Temperature ($^{\circ}\text{C}$)	Small Phytoplankton Biomass (mol P kg^{-1}); Large Phytoplankton Biomass (mol P kg^{-1})	BLING	PI Control; LgSm	Different diagnostic BC across model runs	Nearly identical circulations produced by ESM2Mc
3	Macronutrient (mol kg^{-1}); Micronutrient (mol kg^{-1}); Irradiance (W m^{-2})	Total Phytoplankton Biomass (mol P kg^{-1})	miniBLING and TOPAZ	One model run from miniBLING; one model run from TOPAZ	Simple diagnostic vs complex pronostic BC	Identical physical circulations produced by ocean component of ESM2M

Table 2: The performance metrics for the training and testing subsets for the trained NNEs from each case separated into their respective size classes and ESM/model runs.

Case #	Phytoplankton Size	ESM/Model Run/BC	Training Data		Testing Data	
			R-squared	RMSE	R-squared	RMSE
1	Small Phytoplankton	ESM2Mc / PI Control / BLING	0.9912	6.24×10^{-10}	0.9908	6.35×10^{-10}
		ESM2Mc / 4x CO ₂ / BLING	0.9906	6.18×10^{-10}	0.9903	6.26×10^{-10}
		ESM2Mc / 3x Mixing / BLING	0.9912	6.22×10^{-10}	0.9906	6.35×10^{-10}
	Large Phytoplankton	ESM2Mc / PI Control / BLING	0.9790	3.00×10^{-9}	0.9771	3.11×10^{-9}
		ESM2Mc / 4x CO ₂ / BLING	0.9749	2.74×10^{-9}	0.9740	2.77×10^{-9}
		ESM2Mc / 3x Mixing / BLING	0.9804	3.00×10^{-9}	0.9778	3.11×10^{-9}
2	Small Phytoplankton	ESM2Mc / PI Control / BLING	0.9912	6.24×10^{-10}	0.9908	6.35×10^{-10}
		ESM2Mc / PI Control / BLING-LgSm	0.9762	1.00×10^{-9}	0.9761	1.00×10^{-9}
	Large Phytoplankton	ESM2Mc / PI Control / BLING	0.9790	3.00×10^{-9}	0.9771	3.11×10^{-9}
		ESM2Mc / PI Control / BLING-LgSm	0.9862	2.34×10^{-9}	0.9855	2.38×10^{-9}
3	Total Phytoplankton	ESM2Mo / Historical / miniBLING	0.9511	8.97×10^{-9}	0.9507	9.11×10^{-9}
		ESM2Mo / Historical / TOPAZ	0.5893	8.97×10^{-9}	0.5867	8.99×10^{-9}

Table 3: The performance metrics for the NNEs being used to predict the outcome of the other model runs for the same size class of Case 1. In the top half of the table, the R-squared and RMSE are listed. The values in parentheses are the values from comparing the respective cases against one another (these are the same values listed in the respective scatter plots of Fig. 5 and 6). The values outside the parentheses are the values from using the trained NNE of the model listed in the row to predict the outcome of the model run in the column (e.g., the NNE trained on 4xCO₂ was used to predict the PI Control outcome using the predictor values of PI Control. These values were compared against the actual values of the PI Control to compute the RMSE of 7.15x10⁻¹⁰). In the bottom half of the table is the percent decrease in RMSE from the number listed inside the parentheses to the RMSE outside the parentheses.

			Case being predicted								
			Small Phytoplankton			Large Phytoplankton					
			PI Control	4x CO2	3x Mixing	PI Control	4x CO2	3x Mixing			
R-squared	NNE being used for predicting	Small Phytoplankton	PI Control	-	(0.8290) 0.9874	(0.9287) 0.9902	-	-	-		
			4x CO2	(0.8290) 0.9887	-	(0.7880) 0.9878	-	-	-		
			3x Mixing	(0.9287) 0.9901	(0.7880) 0.9849	-	-	-	-		
		Large Phytoplankton	PI Control	-	-	-	-	(0.7842) 0.9683	(0.8831) 0.9772		
			4x CO2	-	-	-	(0.7842) 0.9722	-	(0.7306) 0.9690		
			3x Mixing	-	-	-	(0.8831) 0.9738	(0.7306) 0.9630	-		
		RMSE	NNE being used for predicting	Small Phytoplankton	PI Control	-	(3.06 x 10 ⁻⁹) 7.38 x 10 ⁻¹⁰	(1.84 x 10 ⁻⁹) 6.55 x 10 ⁻¹⁰	-	-	-
					4x CO2	(3.06 x 10 ⁻⁹) 7.15 x 10 ⁻¹⁰	-	(3.56 x 10 ⁻⁹) 7.30 x 10 ⁻¹⁰	-	-	-
					3x Mixing	(1.84 x 10 ⁻⁹) 6.64 x 10 ⁻¹⁰	(3.56 x 10 ⁻⁹) 7.97 x 10 ⁻¹⁰	-	-	-	-
Large Phytoplankton	PI Control			-	-	-	-	(1.00 x 10 ⁻⁸) 3.11 x 10 ⁻⁹	(7.34 x 10 ⁻⁹) 3.20 x 10 ⁻⁹		
	4x CO2			-	-	-	(1.00 x 10 ⁻⁸) 3.44 x 10 ⁻⁹	-	(1.17 x 10 ⁻⁸) 3.74 x 10 ⁻⁹		
	3x Mixing			-	-	-	(7.34 x 10 ⁻⁹) 3.34 x 10 ⁻⁹	(1.17 x 10 ⁻⁸) 3.33 x 10 ⁻⁹	-		
Percent Decrease in Error	NNE being used for predicting			Small Phytoplankton	PI Control	-	75.90%	64.45%	-	-	-
					4x CO2	76.66%	-	79.53%	-	-	-
					3x Mixing	63.98%	77.64%	-	-	-	-
		Large Phytoplankton	PI Control	-	-	-	-	69.09%	56.32%		
			4x CO2	-	-	-	65.71%	-	67.99%		
			3x Mixing	-	-	-	54.45%	71.50%	-		

Table 4: The performance metrics for the NNEs being used to predict the outcome of the other model runs for the same size class of Case 2. In the top half of the table, the R-squared and RMSE are listed. The values in parentheses are the values from comparing the respective cases against one another (these are the same values listed in the respective scatter plots of Fig. 9 and 10). The values outside the parentheses are the values from using the trained NNE of the model listed in the row to predict the outcome of the model run in the column (e.g., the NNE trained on LgSm was used to predict the PI Control outcome using the predictor values of PI Control. These values were compared against the actual values of the PI Control to compute the RMSE of 3.07×10^{-9}). In the bottom half of the table is the percent decrease in RMSE from the number listed inside the parentheses to the RMSE outside the parentheses (a negative percent means that the error increased).

				Case being predicted			
				Small Phytoplankton		Large Phytoplankton	
				PI Control	LgSm	PI Control	LgSm
R-squared	NNE being used for predicting	Small Phytoplankton	PI Control	-	(0.5591) 0.8192	-	-
			LgSm	(0.5591) 0.7899	-	-	
		Large Phytoplankton	PI Control	-	-	-	(0.8465) 0.9334
			LgSm	-	-	(0.8465) 0.9171	-
RMSE	NNE being used for predicting	Small Phytoplankton	PI Control	-	(4.98×10^{-9}) 3.95×10^{-9}	-	-
			LgSm	(4.98×10^{-9}) 3.07×10^{-9}	-	-	-
		Large Phytoplankton	PI Control	-	-	-	(8.18×10^{-9}) 1.56×10^{-8}
			LgSm	-	-	(8.18×10^{-9}) 1.01×10^{-8}	-
Percent Decrease in Error	NNE being used for predicting	Small Phytoplankton	PI Control	-	20.59%	-	-
			LgSm	38.20%	-	-	-
		Large Phytoplankton	PI Control	-	-	-	-90.87%
			LgSm	-	-	-23.11%	-

Table 5: The performance metrics for the NNEs being used to predict the outcome of the other ESM of Case 3. In the top half of the table, the R-squared and RMSE are listed. The values in paratheses are the values from comparing the respective ESMs against one another (these are the same values listed in the respective scatter plot of Fig. 12). The values outside the parentheses are the values from using the trained NNE of the ESM listed in the row to predict the outcome of the ESM in the column (e.g., the NNE trained on the TOPAZ simulation was used to predict the outcome of the miniBLING using the predictor values computed using the miniBLING simulation. These values were compared against the actual values of the miniBLING simulation to compute the RMSE of 3.91×10^{-8}). In the bottom half of the table is the percent decrease in RMSE from the number listed inside the parentheses to the RMSE outside the parentheses (a negative percent means that the error increased).

			Case being predicted	
			miniBLING	TOPAZ
R-squared	NNE being used for predicting	miniBLING	-	(0.2900) 0.3985
		TOPAZ	(0.2900) 0.5405	-
RMSE	NNE being used for predicting	miniBLING	-	(3.72×10^{-8}) 7.79×10^{-8}
		TOPAZ	(3.72×10^{-8}) 3.91×10^{-8}	-
Percent Decrease in Error	NNE being used for predicting	miniBLING	-	-109.29%
		TOPAZ	-5.03%	-

Table 6: The performance metrics for the training and testing subsets of NNEs trained on different variable combinations of CMIP5 ESM2M output and details about the predictor/target variables.

Variable Groupings	Predictor Variables	Target Variable	Training Data		Testing Data	
			R-squared	RMSE	R-squared	RMSE
All Variables	1) Nitrate (mol m^{-3})	Phytoplankton Concentration (mol N m^{-3})	0.9756	3.61×10^{-5}	0.9754	3.65×10^{-5}
	2) Ammonium (mol m^{-3})					
	3) Phosphate (mol m^{-3})					
	4) Dissolved Iron (mol m^{-3})					
	5) Silicate (mol m^{-3})					
	6) Temperature (K)					
	7) Net Downward Shortwave Flux (W m^{-2})					
	8) Mixed Layer Thickness (m)					
	9) Surface X-Velocity (m s^{-1})					
	10) Surface Y-Velocity (m s^{-1})					
	11) Upward Ocean Mass Transport at 45 m Depth (kg s^{-1})					
Only Variables Directly Affecting Phytoplankton Growth Rate	1) Nitrate (mol m^{-3})	Phytoplankton Concentration (mol N m^{-3})	0.9358	5.87×10^{-5}	0.9352	5.93×10^{-5}
	2) Ammonium (mol m^{-3})					
	3) Phosphate (mol m^{-3})					
	4) Dissolved Iron (mol m^{-3})					
	5) Silicate (mol m^{-3})					
	6) Temperature (K)					
	7) Net Downward Shortwave Flux (W m^{-2})					
Only Variables NOT Directly Affecting Phytoplankton Growth Rate	1) Mixed Layer Thickness (m)	Phytoplankton Concentration (mol N m^{-3})	0.3268	1.90×10^{-4}	0.3279	1.91×10^{-4}
	2) Surface X-Velocity (m s^{-1})					
	3) Surface Y-Velocity (m s^{-1})					
	4) Upward Ocean Mass Transport at 45 m Depth (kg s^{-1})					

Figures

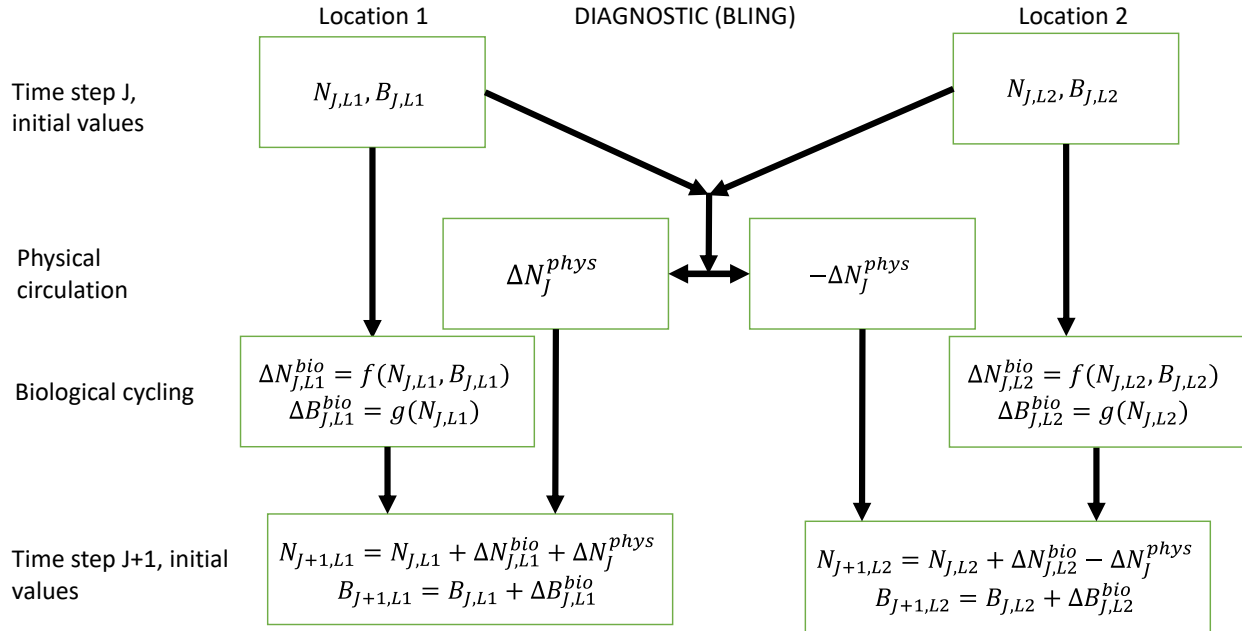


Figure 1: Conceptual diagram of how biogeochemical evolution is computed within an ESM using the BLING BC. The letters and abbreviations represent: nutrients (N), phytoplankton biomass (B), the physical circulation component (phys), and the biological cycling component (bio). Each location has initial values for nutrients and biomass. These initial values are passed to the intrinsic biological relationships which then feed into the g function in the biological cycling box that are then used to calculate the changes in nutrients and biomass due to biological cycling. The initial nutrient concentrations between the two locations result in a change in nutrients from physical transport, which is equal in magnitude and opposite in sign between the two boxes (physical circulation component). When the physical circulation and biological cycling portions are coupled together, the nutrients and biomass for the next time step are calculated.

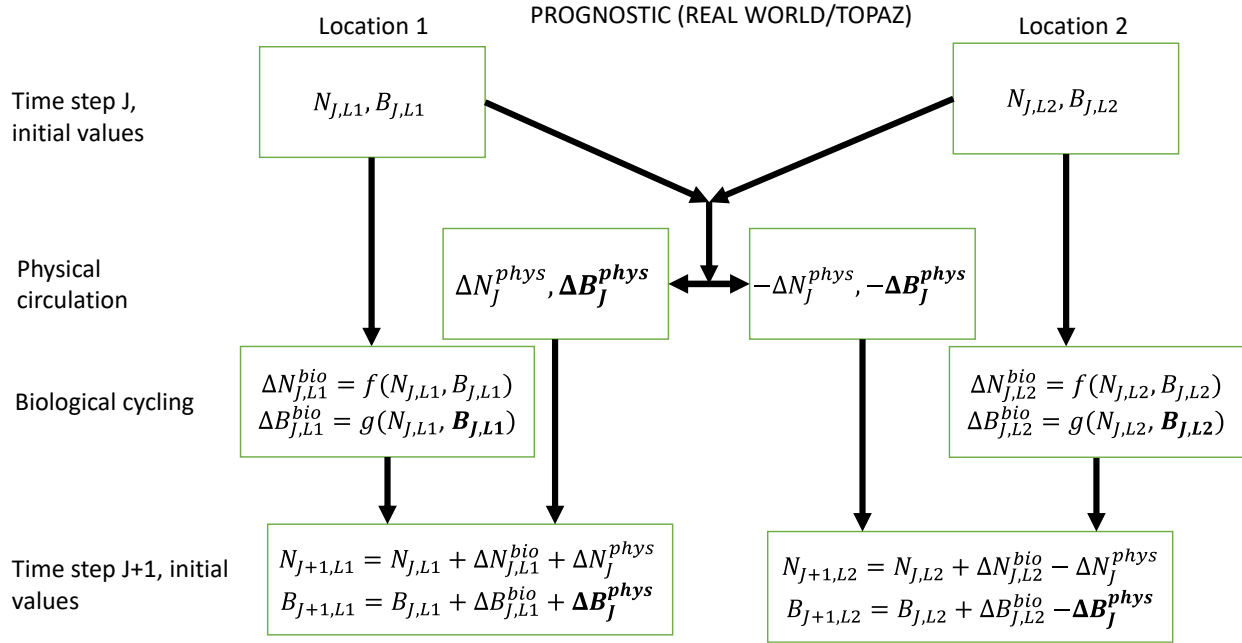


Figure 2: Conceptual diagram of how biogeochemical evolution is computed within an ESM using the prognostic TOPAZ BC. The letters and abbreviations represent: nutrients (N), phytoplankton biomass (B), the physical circulation component (phys), and the biological cycling component (bio). This ESM differs from the one described in Fig. 1. In this prognostic model, the changes in biomass from the biological cycling component are a function of the nutrients and biomass, rather than nutrients alone. Additionally, a change in biomass due to physical circulation is added.

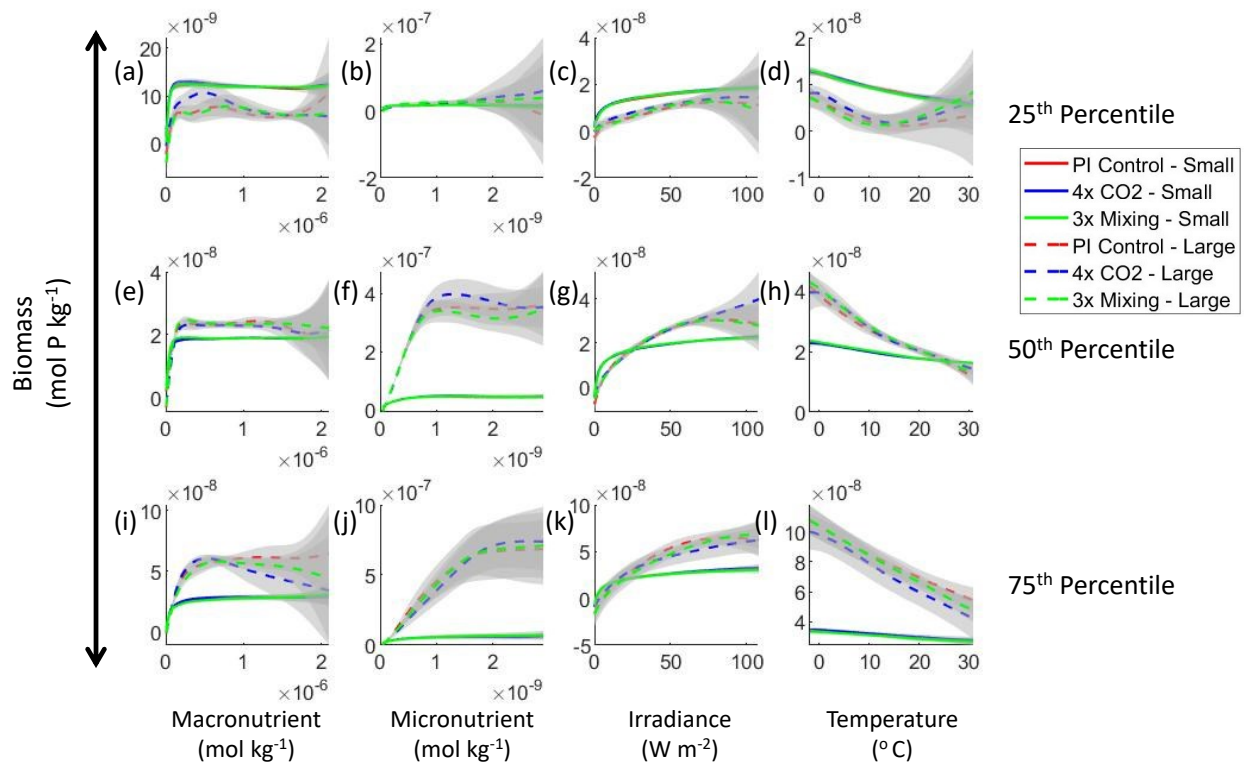


Figure 3: Sensitivity analysis plots for the small and large phytoplankton of Case 1. Each line is the prediction for the NNE (i.e., the average prediction of 25 NNs) specific to each model run and the color of each line represents the model run (PI Control – Red; 4xCO₂ – Blue; 3xMixing - Green). The solid lines correspond to the NNE predictions for small phytoplankton and the dashed lines to the NNE predictions for large phytoplankton. The gray region around each line shows one standard deviation in the predictions of the individual NNs that make up each NNE (e.g., the gray region around the solid red curves shows the standard deviation in the predictions of the 25 NNs that make up that particular NNE). The rows correspond to the percentile value at which the other predictor variables are held constant (e.g., box (a) varies the macronutrient across its min-max range and holds the micronutrient, irradiance, and temperature at their respective 25th percentile values). Columns show the x-axis variables as they vary between their min-max range. The y-axis in all subplots is the biomass concentration. Note that the biomass scale changes with each subplot.

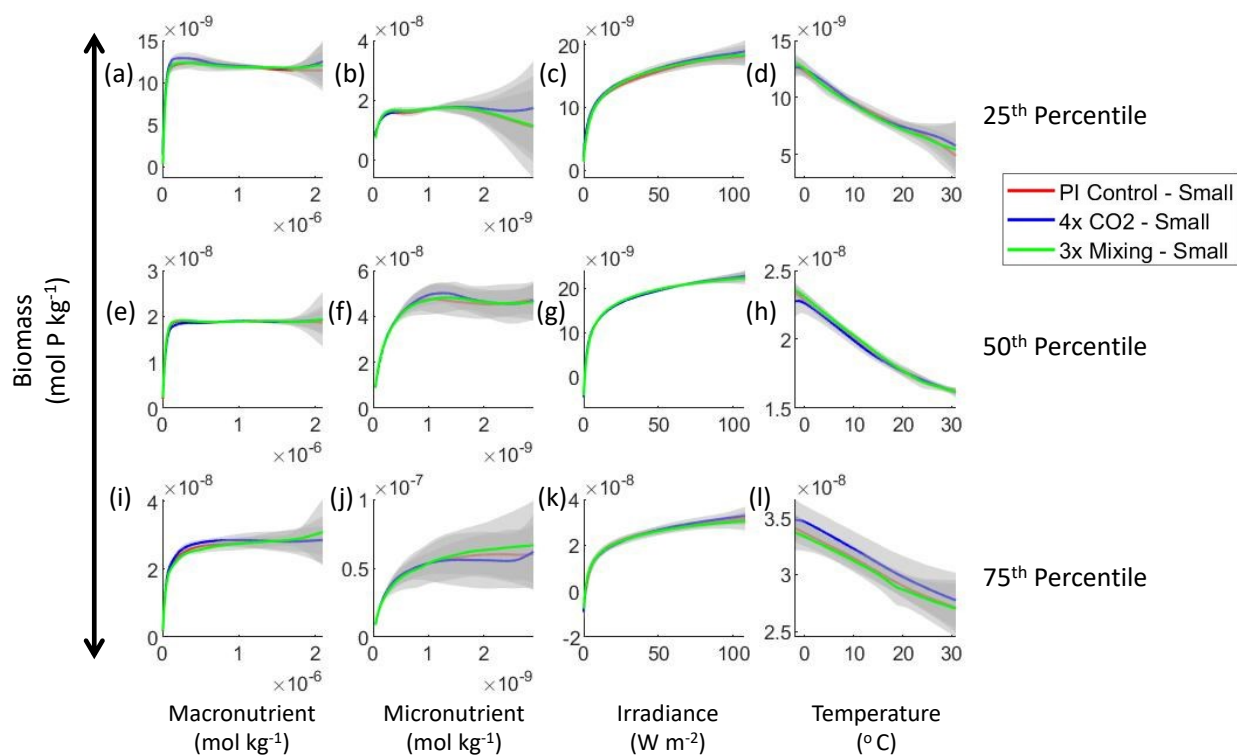


Figure 4: Sensitivity analysis plots for the small phytoplankton of Case 1. This figure is provided to allow for examination of the apparent relationships for the small phytoplankton, since the large phytoplankton apparent relationships made it difficult to see those for the small phytoplankton in Fig. 3. Each line is the prediction for the NNE (i.e., the average prediction of 25 NNs) specific to each model run and the color of each line represents the model run (PI Control – Red; 4xCO₂ – Blue; 3xMixing - Green). The gray region around each line shows one standard deviation in the predictions of the individual NNs that make up each NNE (e.g., the gray region around the solid red curves shows the standard deviation in the predictions of the 25 NNs that make up that particular NNE). The rows correspond to the percentile value at which the other predictor variables were held constant (e.g., box (a) varies the macronutrient across its min-max range and holds the micronutrient, irradiance, and temperature at their respective 25th percentile values). Columns show the x-axis variables as they vary between their min-max range. The y-axis in all subplots is the biomass concentration. Note that the biomass scale changes with each subplot.

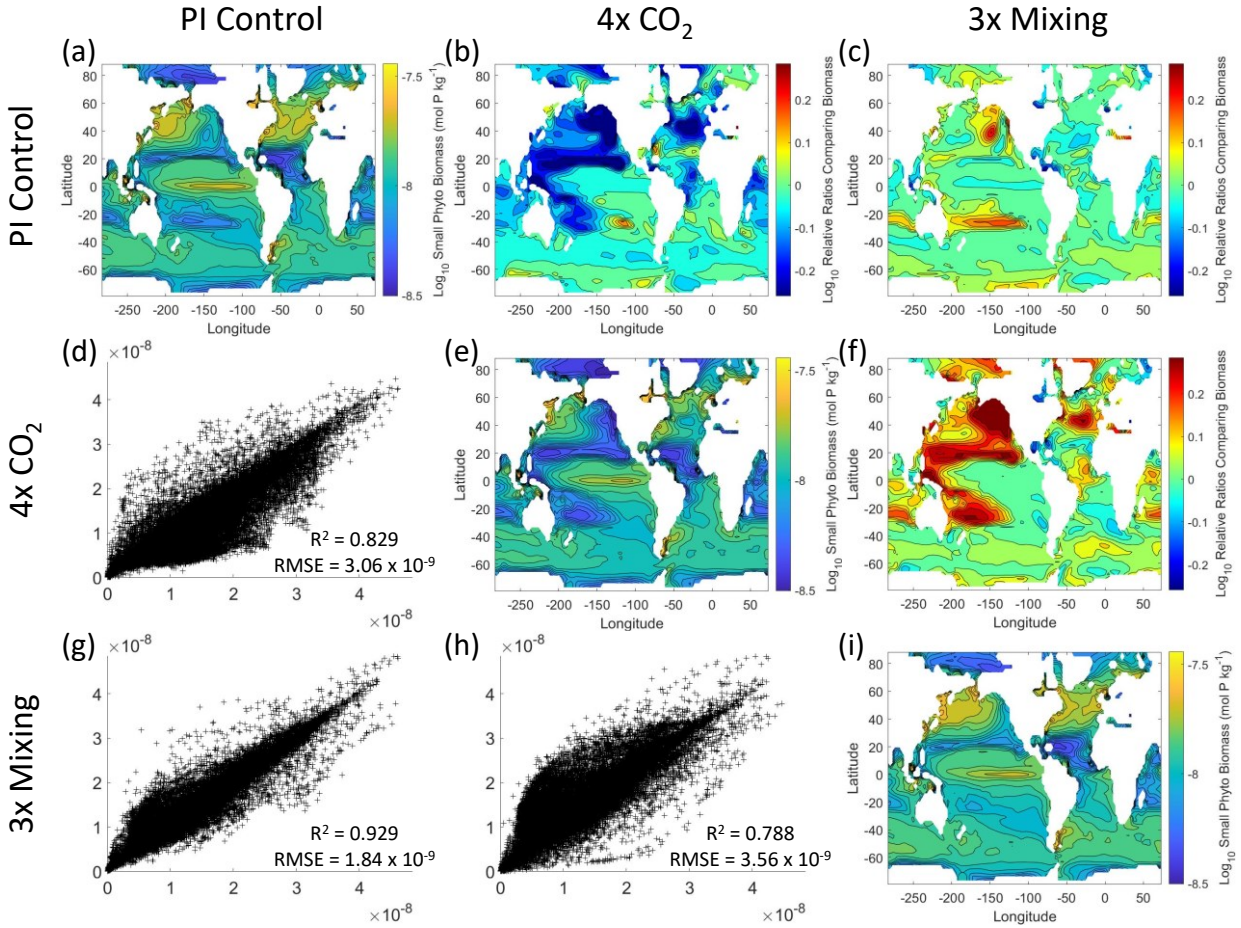


Figure 5: Comparison of the model runs for small phytoplankton biomass in Case 1. The units for biomass in all subplots are mol P kg⁻¹. The subplots show point-by-point scatter plots comparing the model runs against one another (d, g, h), yearly averaged log₁₀ biomass plots for each model run (a, e, i), and the log₁₀ relative ratios comparing the yearly averaged contour plots of the model runs (b, c, f). The x-axis and y-axis of the scatter plots (d, g, h) correspond to the horizontal/vertical model run labels, respectively (e.g., box (d) shows PI Control on the x-axis and 4xCO₂ on the y-axis). The yearly averaged log₁₀ contour plots (a, e, i) correspond to the matching horizontal/vertical model run labels (e.g., box (a) shows the yearly averaged log₁₀ biomass of PI Control). The log₁₀ relative ratios (b, c, f) were calculated as the model run listed on the horizontal axis divided by the model run listed on the vertical axis (e.g., box (b) shows 4xCO₂ divided PI Control).

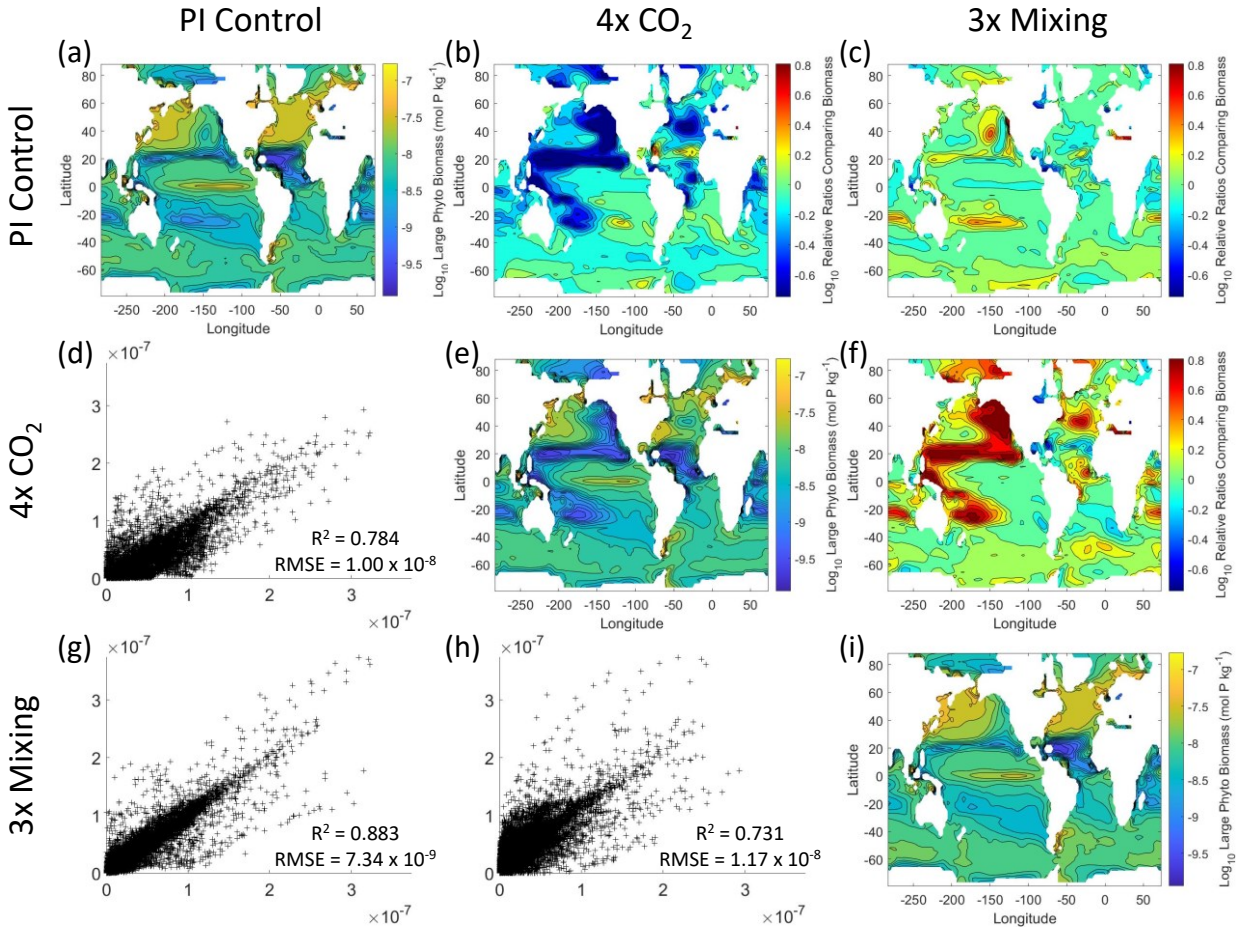


Figure 6: Comparison of the model runs for large phytoplankton biomass in Case 1. The units for biomass in all subplots are mol P kg⁻¹. The subplots show point-by-point scatter plots comparing the model runs against one another (d, g, h), yearly averaged log₁₀ biomass plots for each model run (a, e, i), and the log₁₀ relative ratios comparing the yearly averaged contour plots of the model runs (b, c, f). The x-axis and y-axis of the scatter plots (d, g, h) correspond to the horizontal/vertical model run labels, respectively (e.g., box (d) shows PI Control on the x-axis and 4xCO₂ on the y-axis). The yearly averaged log₁₀ contour plots (a, e, i) correspond to the matching horizontal/vertical model run labels (e.g., box (a) shows the yearly averaged log₁₀ biomass of PI Control). The log₁₀ relative ratios (b, c, f) were calculated as the model run listed on the horizontal axis divided by the model run listed on the vertical axis (e.g., box (b) shows 4xCO₂ divided PI Control).

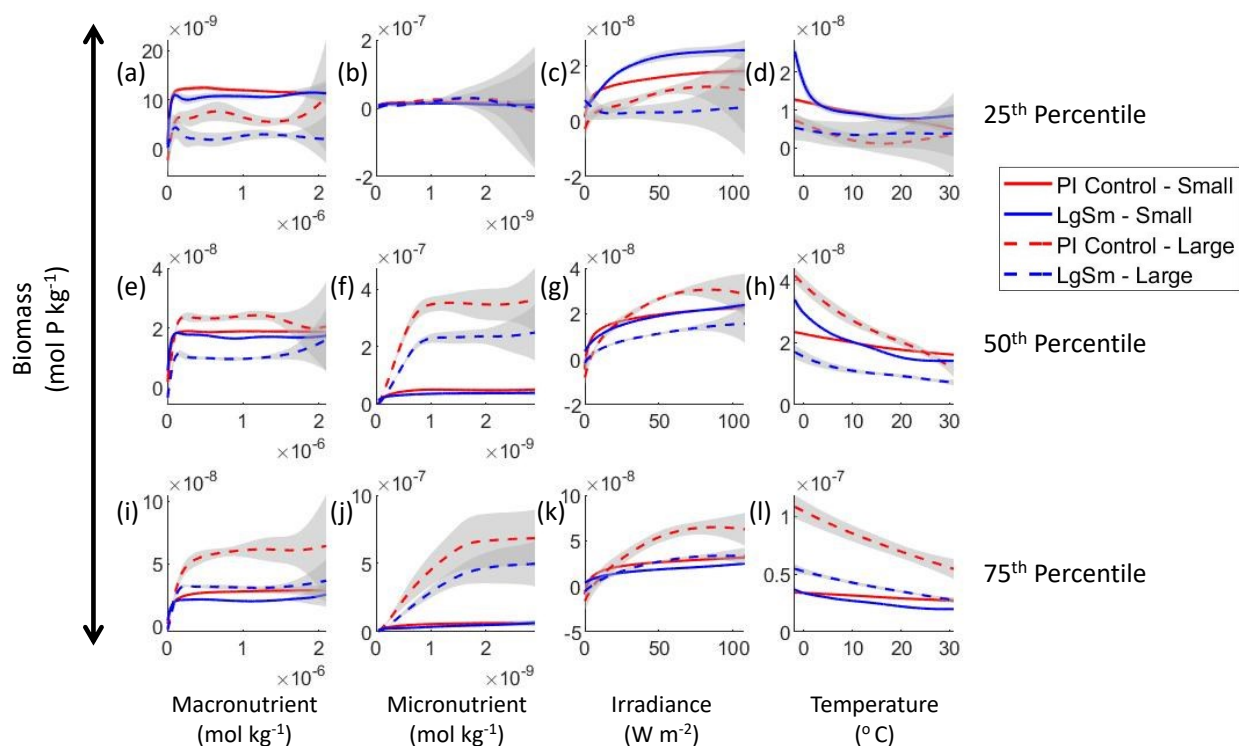


Figure 7: Sensitivity analysis plots for the small and large phytoplankton of Case 2. Each line is the prediction for the NNE (i.e., the average prediction of 25 NNs) specific to each model run and the color of each line represents the model run (PI Control – Red; LgSm – Blue). The solid lines correspond to the small phytoplankton and the dashed lines to the large phytoplankton. The gray region around each line shows one standard deviation in the predictions of the individual NNs that make up each NNE (e.g., the gray region around the solid red curves shows the standard deviation in the predictions of the 25 NNs that make up that particular NNE). The rows correspond to the percentile value at which the other predictor variables were held constant (e.g., box (a) varies the macronutrient across its min-max range and holds the micronutrient, irradiance, and temperature at their respective 25th percentile values). Columns show the x-axis variables as they vary between their min-max range. The y-axis in all subplots is the biomass concentration. Note that the biomass scale changes with each subplot.

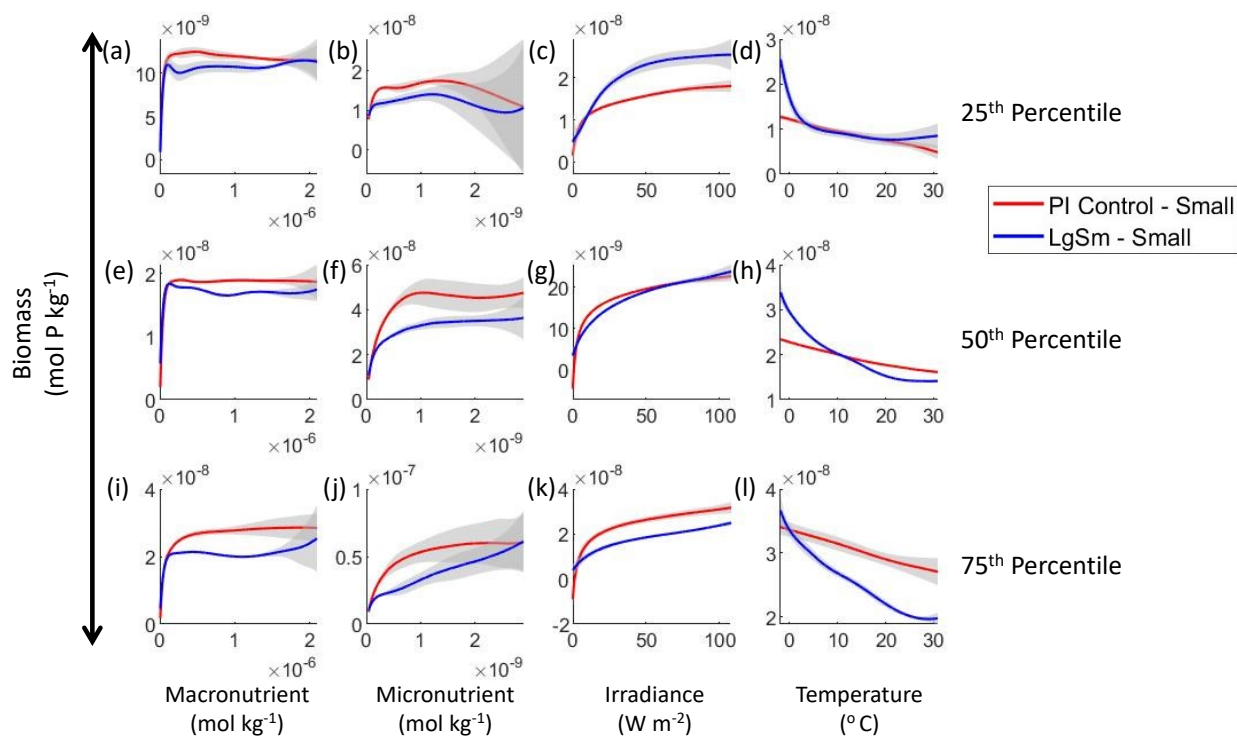


Figure 8: Sensitivity analysis plots for the small phytoplankton of Case 2. This figure is provided to allow for examination of the apparent relationships for the small phytoplankton, since the large phytoplankton apparent relationships made it difficult to see those for the small phytoplankton in Fig. 7. Each line is the prediction for the NNE (i.e., the average prediction of 25 NNs) specific to each model run and the color of each line represents the model run (PI Control – Red; LgSm – Blue). The gray region around each line shows one standard deviation in the predictions of the individual NNs that make up each NNE (e.g., the gray region around the solid red curves shows the standard deviation in the predictions of the 25 NNs that make up that particular NNE). The rows correspond to the percentile value at which the other predictor variables were held constant (e.g., box (a) varies the macronutrient across its min-max range and holds the micronutrient, irradiance, and temperature at their respective 25th percentile values). Columns show the x-axis variables as they vary between their min-max range. The y-axis in all subplots is the biomass concentration. Note that the biomass scale changes with each subplot.

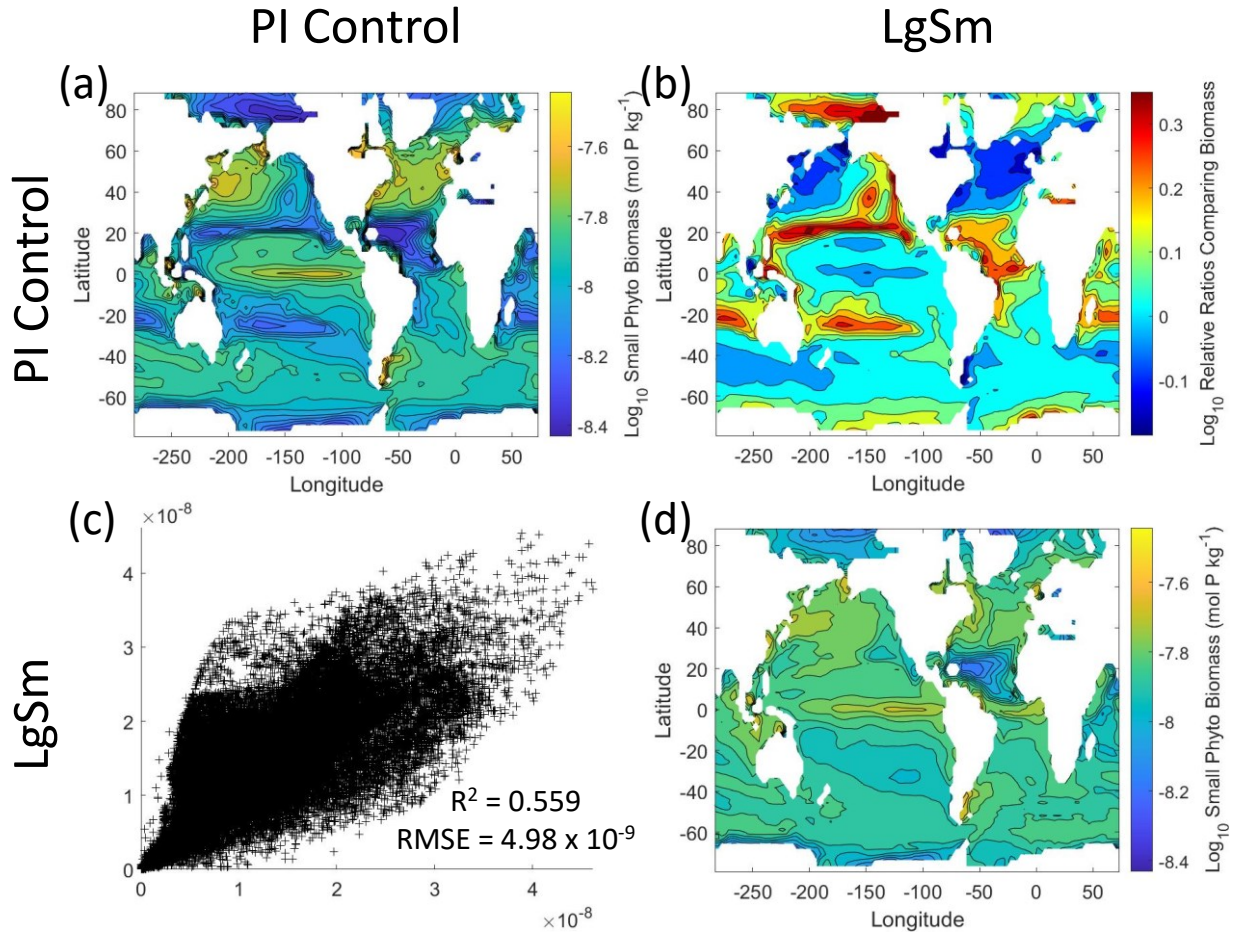


Figure 9: Comparison of the model runs for small phytoplankton biomass in Case 2. The units for biomass in all subplots are mol P kg^{-1} . The subplots show point-by-point scatter plots comparing the model runs against one another (c), yearly averaged log_{10} biomass plots for each model run (a and d), and the log_{10} relative ratios comparing the yearly averaged contour plots of the model runs (b). The x-axis and y-axis of the scatter plots (c) correspond to the horizontal/vertical model run labels, respectively (e.g., box (c) shows PI Control on the x-axis and LgSm on the y-axis). The yearly averaged log_{10} contour plots (a and d) correspond to the matching horizontal/vertical model run labels (e.g., box (a) shows the yearly averaged log_{10} biomass of PI Control). The log_{10} relative ratios (b) were calculated as the model run listed on the horizontal axis divided by the model run listed on the vertical axis (e.g., box (b) shows LgSm divided PI Control).

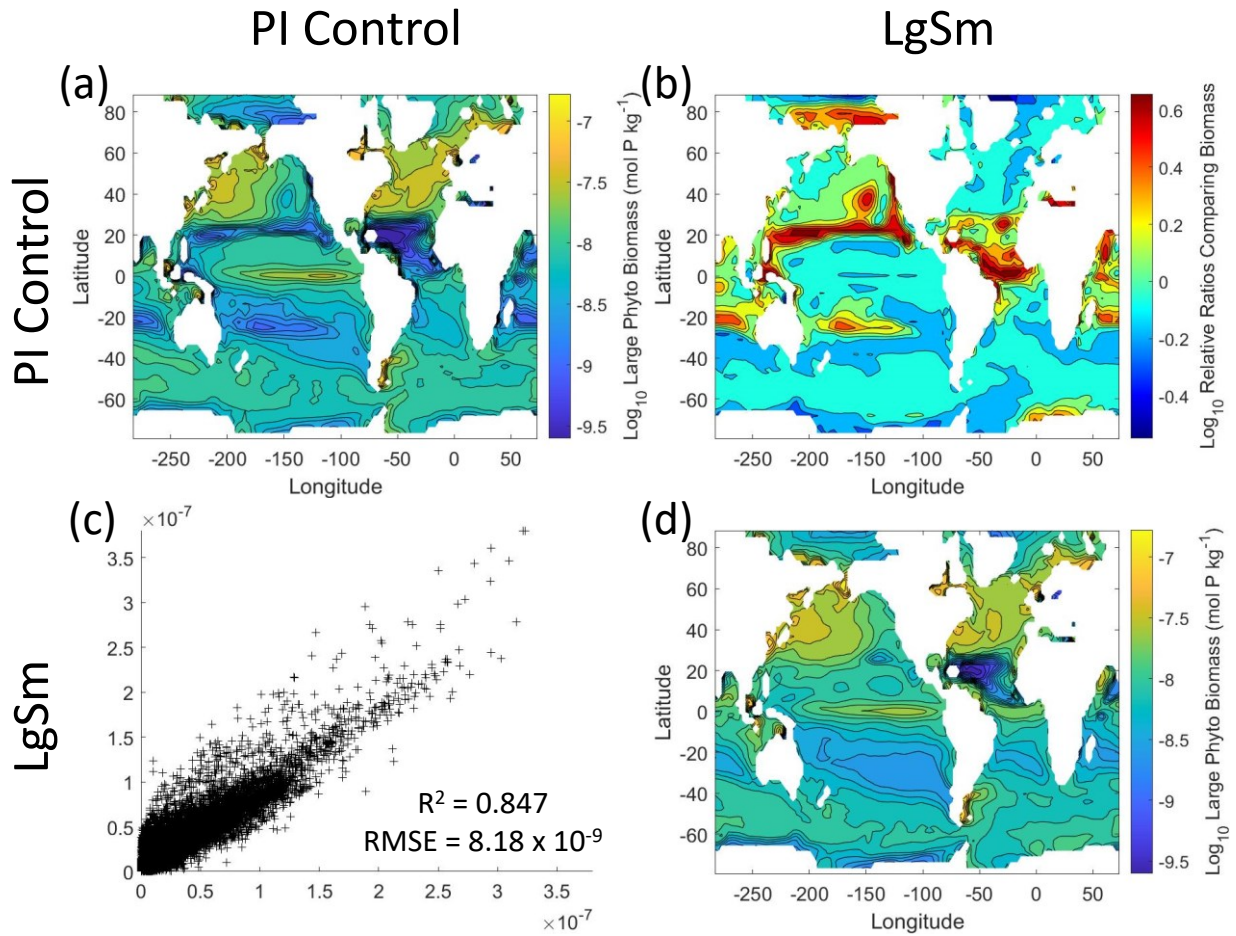


Figure 10: Comparison of the model runs for large phytoplankton biomass in Case 2. The units for biomass in all subplots are mol P kg^{-1} . The subplots show point-by-point scatter plots comparing the model runs against one another (c), yearly averaged log_{10} biomass plots for each model run (a and d), and the log_{10} relative ratios comparing the yearly averaged contour plots of the model runs (b). The x-axis and y-axis of the scatter plots (c) correspond to the horizontal/vertical model run labels, respectively (e.g., box (c) shows PI Control on the x-axis and LgSm on the y-axis). The yearly averaged log_{10} contour plots (a and d) correspond to the matching horizontal/vertical model run labels (e.g., box (a) shows the yearly averaged log_{10} biomass of PI Control). The log_{10} relative ratios (b) were calculated as the model run listed on the horizontal axis divided by the model run listed on the vertical axis (e.g., box (b) shows LgSm divided PI Control).

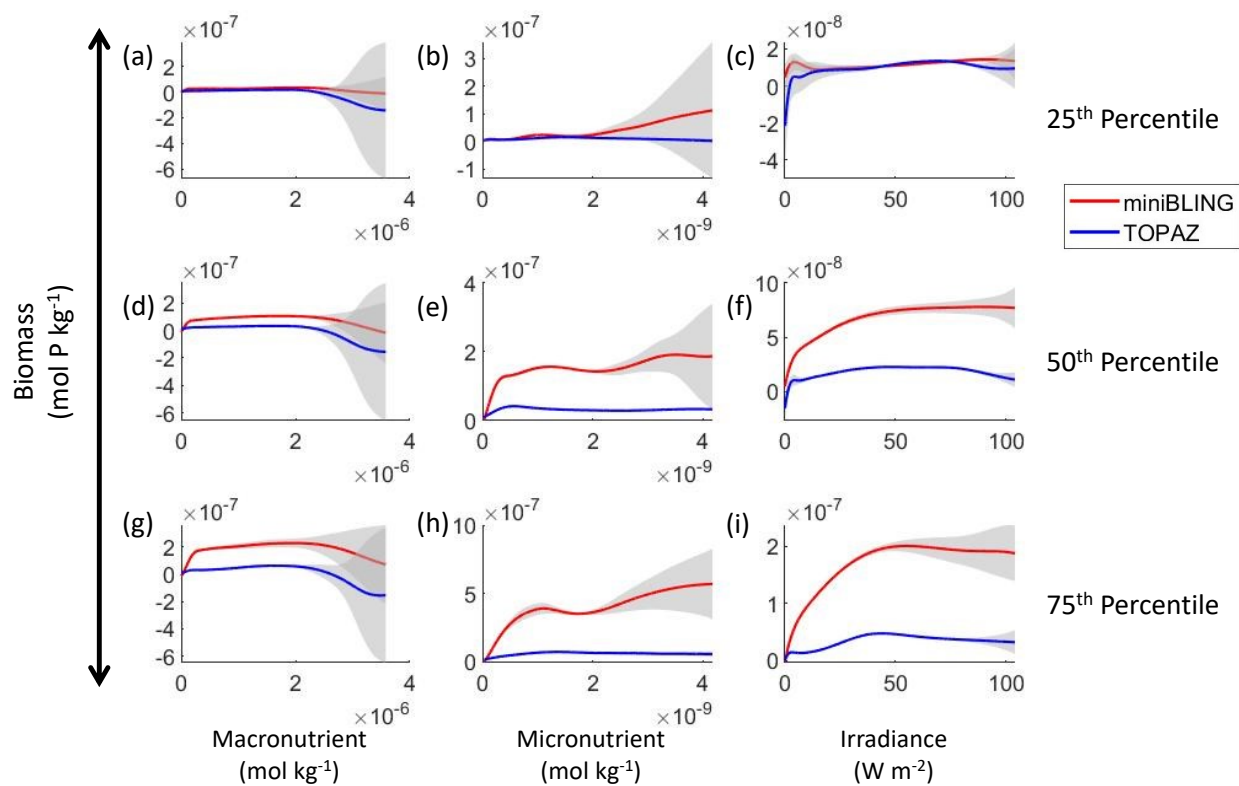


Figure 11: Sensitivity analysis plots for phytoplankton biomass for Case 3. Each line is the prediction for the NNE (i.e., the average prediction of 25 NNs) specific to each ESM and the color of each line represents the ESM (miniBLING – Red; TOPAZ – Blue). The gray region around each line shows one standard deviation in the predictions of the individual NNs that make up each NNE (e.g., the gray region around the solid red curves shows the standard deviation in the predictions of the 25 NNs that make up that particular NNE). The rows correspond to the percentile value at which the other predictor variables were held constant (e.g., box (a) varies the macronutrient across its min-max range and holds the micronutrient and irradiance at their respective 25th percentile values). Columns show the x-axis variables as they vary between their min-max range. The y-axis in all subplots is the biomass concentration. Note that the biomass scale changes with each subplot.

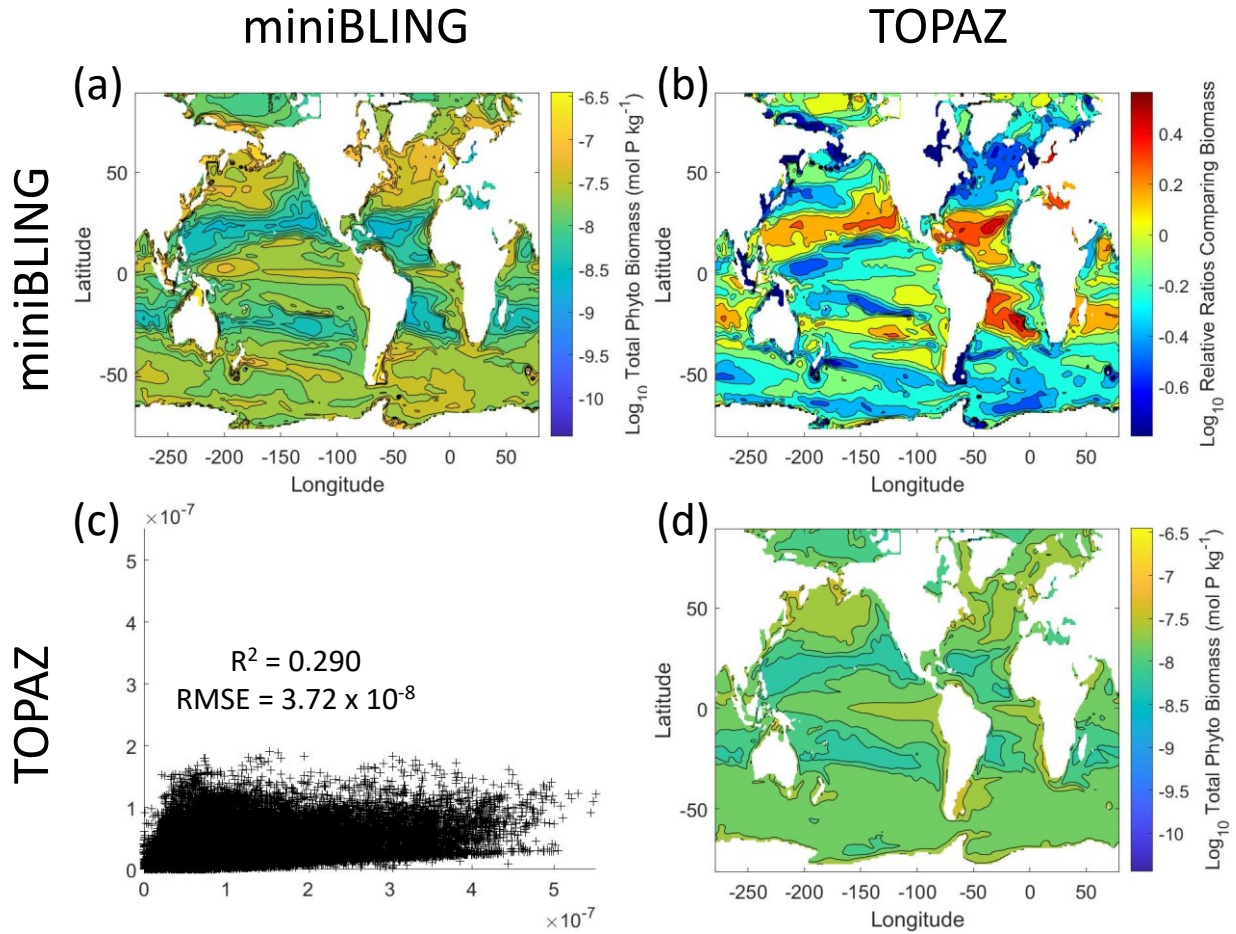


Figure 12: Comparison of the ESMs for total phytoplankton biomass in Case 3 in which circulation is given by ESM2Mo, but the BCs are different. The units for biomass in all subplots are mol P kg^{-1} . The subplots show point-by-point scatter plots comparing the ESMs against one another (c), yearly averaged \log_{10} biomass plots for each ESM (a and d), and the \log_{10} relative ratios comparing the yearly averaged contour plots of the ESMs (b). The x-axis and y-axis of the scatter plots (c) correspond to the horizontal/vertical ESM labels, respectively (e.g., box (c) shows the miniBLING simulation on the x-axis and the TOPAZ simulation on the y-axis). The yearly averaged \log_{10} contour plots (a and d) correspond to the matching horizontal/vertical ESM labels (e.g., box (a) shows the yearly averaged \log_{10} biomass of miniBLING). The \log_{10} relative ratios (b) were calculated as the ESM listed on the horizontal axis divided by the ESM listed on the vertical axis (e.g., box (b) shows TOPAZ divided by miniBLING).